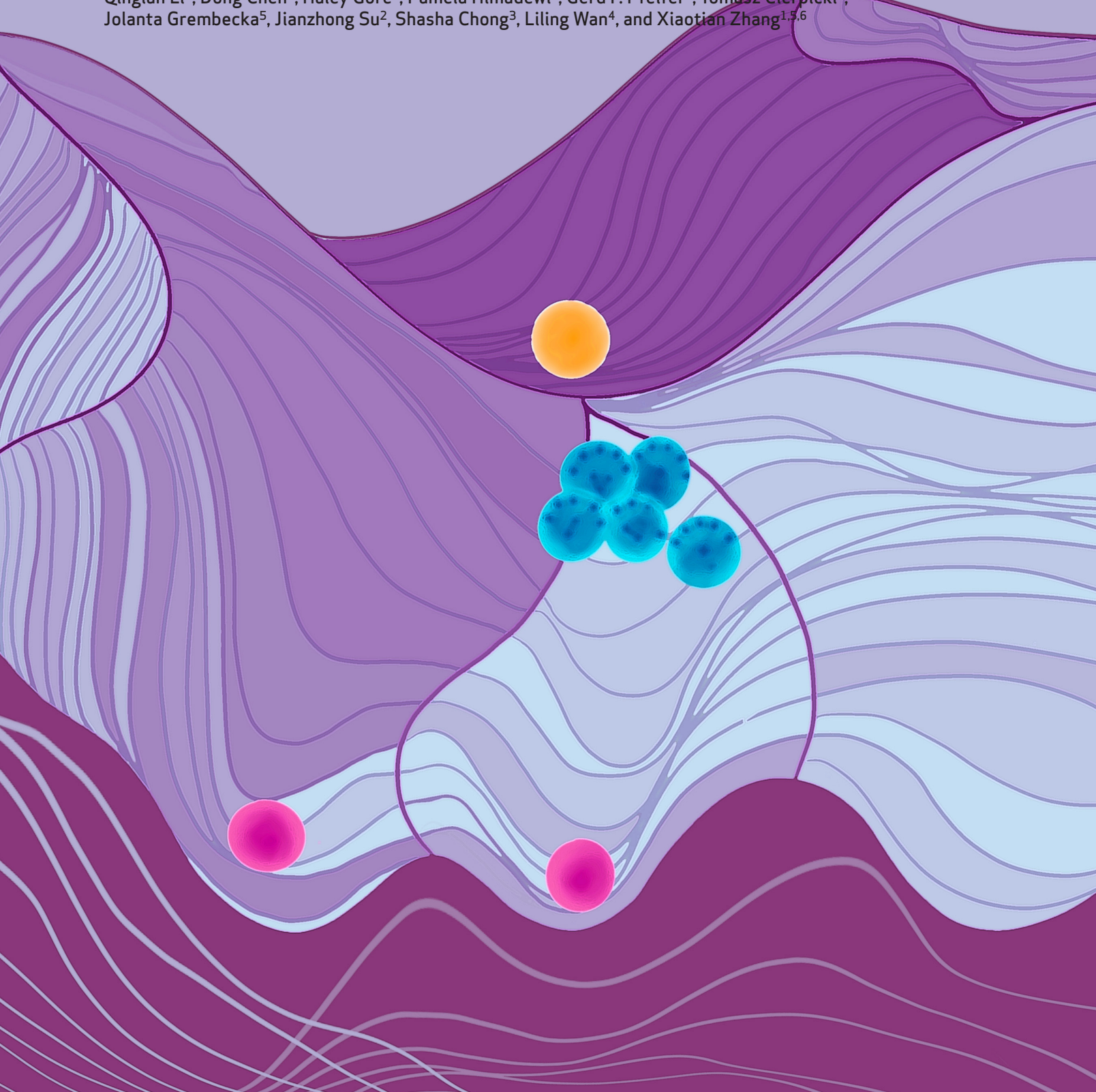


Mutant NPM1 Hijacks Transcriptional Hubs to Maintain Pathogenic Gene Programs in Acute Myeloid Leukemia



Xue Qing David Wang¹, Dandan Fan², Qinyu Han³, Yiman Liu⁴, Hongzhi Miao⁵, Xinyu Wang², Qinglan Li³, Dong Chen⁵, Haley Gore¹, Pamela Himadewi¹, Gerd P. Pfeifer¹, Tomasz Cierpicki⁵, Jolanta Grembecka⁵, Jianzhong Su², Shasha Chong³, Liling Wan⁴, and Xiaotian Zhang^{1,5,6}



ABSTRACT

Nucleophosmin (NPM1) is a ubiquitously expressed nucleolar protein with a wide range of biological functions. In 30% of acute myeloid leukemia (AML), the terminal exon of *NPM1* is often found mutated, resulting in the addition of a nuclear export signal and a shift of the protein to the cytoplasm (NPM1c). AMLs carrying this mutation have aberrant expression of the *HOXA/B* genes, whose overexpression leads to leukemogenic transformation. Here, for the first time, we comprehensively prove that NPM1c binds to a subset of active gene promoters in NPM1c AMLs, including well-known leukemia-driving genes—*HOXA/B* cluster genes and *MEIS1*. NPM1c sustains the active transcription of key target genes by orchestrating a transcription hub and maintains the active chromatin landscape by inhibiting the activity of histone deacetylases. Together, these findings reveal the neomorphic function of NPM1c as a transcriptional amplifier for leukemic gene expression and open up new paradigms for therapeutic intervention.

SIGNIFICANCE: *NPM1* mutation is the most common mutation in AML, yet the mechanism of how the mutant protein results in AML remains unclear. Here, for the first time, we prove mutant NPM1 directly binds to active chromatin regions and hijacks the transcription of AML-driving genes.

See related article by Uckelmann et al., p. 746.

INTRODUCTION

NPM1 is a multifunctional nucleolar protein involved in ribosome biogenesis, ribosomal RNA (rRNA) transcription, centromere maintenance, and histone chaperone activity (1–6). It contains an intrinsic disorder region (IDR) and participates in the formation of nucleolus with multivalent homotypic and heterotypic interactions with RNA and other nucleolar proteins by liquid–liquid phase separation (LLPS; refs. 7, 8). In acute myeloid leukemia (AML), a four-base pair insertion in the last exon of *NPM1* results in a mutant NPM1 protein with an additional nuclear export signal (NES; refs. 2, 9). Mutant NPM1 protein (NPM1c) translocates from

the nucleolus to the cytoplasm and activates the *HOXA/B* cluster genes in AML (10–12).

Multiple hypotheses have been proposed to explain the mutant NPM1c's function in the transformation of normal hematopoietic stem and progenitor cells (HSPC). Data from genetically engineered mouse models suggest that *Npm1* heterozygosity induces myeloid dysplasia, and transgenic expression of *Npm1c* or conditional knockin of *Npm1c* in hematopoietic lineage results in AML development in mice (12–15). This difference in the disease spectrum of these mouse models suggests that *NPM1c* mutation, not the loss of *NPM1*, is required for AML development. Yet, the exact molecular mechanism of *HOXA/B* cluster gene activation by NPM1c remains unclear. Various data suggest the sequestration of *HOXA/B* repressor elements to the cytoplasm by the transitioning NPM1c (16–19). As such, these proposed models suggest that NPM1c functions as a derepressor of transcriptionally silent genes. Other data suggest that NPM1c or NPM1 wild-type (WT) protein can directly regulate the gene expression through an unidentified, but potentially chromatin-associated mechanism (20–25). These data suggest that NPM1c and/or NPM1-WT are direct activators of gene expression. Given the conflicting data, thus far, no study has comprehensively delineated how NPM1c modulates gene expression. Particularly, no research has been performed on the nature of *NPM1c* mutation. Whether the effects on gene expression are attributed to *NPM1* haploinsufficiency, or NPM1c has a neomorphic function, is unknown. Importantly, whether NPM1-WT and/or NPM1c plays a role in the aberrant expression of key leukemic genes such as *HOXA/B* cluster genes and *MEIS1* in NPM1c⁺ AMLs remains unclear. This opacity hinders the study of the mechanism on NPM1c driving leukemia transformation and the development of novel therapy.

Here, for the first time, we comprehensively prove that NPM1c, not NPM1-WT, binds to active chromatin regions marked by H3K27ac in NPM1c⁺ AML cell lines and primary blasts. Chromatin-bound NPM1c directly modulates the active nascent transcription of leukemia-driving

¹Department of Epigenetics, Van Andel Research Institute, Grand Rapids, Michigan. ²Institute of Biomedical Big Data, Wenzhou Medical University, Wenzhou, China. ³Division of Chemistry and Chemical Engineering, California Institute of Technology, Pasadena, California. ⁴Department of Cancer Biology and Abramson Family Cancer Research Institute, Perelman School of Medicine, University of Pennsylvania, Philadelphia, Pennsylvania. ⁵Department of Pathology, University of Michigan, Ann Arbor, Michigan. ⁶Department of Biochemistry and Molecular Biology, University of Texas Health Science Center at Houston, McGovern Medical School, Houston, Texas.

Note: X.Q.D. Wang, D. Fan, Q. Han, and Y. Liu contributed equally to this article. J. Su, S. Chong, L. Wan, and X. Zhang jointly supervised this article.

Current address for X.Q.D. Wang: Department of Biochemistry, University of Southern California, Los Angeles, California.

Corresponding Authors: Xiaotian Zhang, University of Texas Health Science Center at Houston, Room MSB6.202, 6431 Fannin Street, Houston, TX 77030. Phone: 713-500-5146; E-mail: Xiaotian.Zhang@uth.tmc.edu; Liling Wan, University of Pennsylvania, BRB II/III, RM751, 421 Curie Boulevard, Philadelphia, PA 19104. Phone: 215-898-3116; E-mail: liling.wan@penmedicine.upenn.edu; and Shasha Chong, California Institute of Technology, 1200 East California Boulevard, MC 147-75, Pasadena, CA 91125. Phone: 626-395-5736; E-mail: schong@caltech.edu
Cancer Discov 2023;13:724–45

doi: 10.1158/2159-8290.CD-22-0424

This open access article is distributed under the Creative Commons Attribution-NonCommercial-NoDerivatives 4.0 International (CC BY-NC-ND 4.0) license.

©2022 The Authors; Published by the American Association for Cancer Research

genes—*HOXA/B* cluster genes and *MEIS1*. It hijacks the active transcription by concentrating the transcriptional complexes [RNA polymerase II (Pol II), MLL–Menin complex, and super elongation complex (SEC)] at target loci through multivalent heterotypic interactions. Such a hijacking by NPM1c in AML also maintains the active chromatin state at target gene loci by repelling repressive histone deacetylases (HDAC), which mediates the silencing of *HOXA/B* cluster genes and *MEIS1* during myeloid differentiation. We find that NPM1c's transcriptional targets are cell-type specific and depend on the active transcription in the cell of origin carrying the NPM1c mutation. Importantly, we find NPM1c's chromatin enrichment depends on the interactions with the nuclear export protein XPO1. We disrupted NPM1c's chromatin binding and transcriptional hijacking by using a clinical-grade XPO1 inhibitor. Furthermore, by combining Menin and XPO1 inhibitors, we achieved significant cell differentiation and leukemia-driving gene downregulation in NPM1c AML. Our data reveal a novel, neomorphic transcription modulation mechanism by NPM1c in leukemia maintenance. Our systematic dissection of NPM1c's transcription hijacking mechanism will lead to a better understanding of transcriptional dysregulation by IDR-containing proteins in cancer and the development of future therapies.

RESULTS

NPM1c Binds to Active Chromatin Regions

Although the function of WT NPM1 protein has been originally characterized within the cell nucleolus, a recent CUT&RUN experiment has shown binding of NPM1-WT at major satellite repeat regions across the genome (bioRxiv 2019.09.27.784835). This revelation led us to hypothesize that NPM1c and/or NPM1-WT protein could bind to chromatin and serve as trans-acting regulatory factors. To evaluate the differences between the two proteins, we used antibodies targeting the C-terminal ends of NPM1c and NPM1-WT, which can distinguish the two proteins across both immunofluorescence and immunoblot assays, to perform CUT&RUN and elucidate the chromatin enrichment profile of the respective proteins in the OCI-AML3 NPM1c degren 2 cell line (Fig. 1A; Supplementary Fig. S1A–S1C; ref. 23). This engineered cell line carries an NPM1c protein tagged with FKBP12^{F36V} (FKBP12). This allows the rapid degradation of NPM1c by the dTAG-13–recruited cereblon E3 ubiquitin ligase complex in 6 hours and leads to a rapid downregulation of canonical NPM1c-associated leukemic genes such as *HOXA9*, *HOXB4*, and *MEIS1* (Fig. 1B and C; ref. 10). We validated NPM1c and NPM1-WT enrichment to chromatin in the OCI-AML3 NPM1c degren 2 cell line via immunoblotting the respective proteins following chromatin fractionation (Supplementary Fig. S1D). Using structured illumination microscopy, we also found NPM1c forming small puncta at the nucleus and cytoplasm with the median diameter around 195 nm (Supplementary Fig. S1E and S1F). Aligning the NPM1-WT CUT&RUN reads to the gapless CHM13-T2T human genome, we found NPM1-WT bound to the rRNA gene locus in both NPM1c⁺ and NPM1c[−] leukemia cell lines (Supplementary Fig. S1G and S1H). In contrast, the mutant NPM1c did not bind to the rRNA gene locus (Supplementary

Fig. S1G and S1H). Surprisingly, we observed NPM1c bound to nonrepetitive genomic regions despite its predominant cytoplasmic localization. NPM1c was enriched to the posterior *HOXA* cluster, the *HOXB* cluster, as well as the *MEIS1* gene with a high signal-to-noise ratio (Fig. 1D; Supplementary Fig. S1I). In contrast, NPM1-WT did not bind to these regions (Fig. 1D; Supplementary Fig. S1I). A similar binding profile to the *HOXA/B* clusters and *MEIS1* gene was observed in NPM1c⁺ primary leukemia blasts with various comutation in genes such as *FLT3-ITD*, *DNMT3A*, *IDH1*, and *WT1* (Fig. 1D; Supplementary Fig. S1I). Importantly, the binding to these loci decreased significantly when the OCI-AML3 NPM1c degren 2 cells were treated with dTAG-13, validating the chromatin enrichment ability of NPM1c protein (Fig. 1D; Supplementary Fig. S1B and S1I). In genome-wide analysis, high-confidence NPM1c peaks strongly overlapped activating H3K27ac marks at 6,312 genes (Fig. 1E; Supplementary Table S1). Meanwhile, the repressive H3K27me3 mark was excluded from the NPM1c binding regions (Fig. 1E). This trend of NPM1c colocalization with the active histone mark was also observed in NPM1c⁺ primary blast cells (Fig. 1F). We performed rank ordering of NPM1c binding sites using a super-enhancer detection algorithm and observed super-peaks at known NPM1c-regulated genes such as the *HOXA/B* cluster genes and *MEIS1* (Supplementary Fig. S1J; refs. 26, 27).

Next, we investigated the relationship between NPM1c's loss of chromatin enrichment and gene expression alteration following NPM1c degradation. Although we found genome-wide loss of NPM1c binding following dTAG-13 treatment for 24 hours, this only led to the downregulation of 171 genes and upregulation of 141 genes (Fig. 1G; Supplementary Fig. S1K and S1L; Supplementary Table S2). Further analysis showed that most peaks ($n = 2017$) were lost significantly (>1.5-fold) after dTAG-13 treatment (Supplementary Fig. S2A). Most genes that lost NPM1c binding did not display any gene expression alterations, but for the ones that met the criteria of differential expression, over 90% were downregulated (Supplementary Fig. S2B). Next, we examined if the gene expression level can be correlated with NPM1c's chromatin enrichment strength. We found that the top 3% of genes in the NPM1c chromatin enrichment signal displayed a broad distribution of both NPM1c and H3K27ac spreading to the gene body (Fig. 1G). These top 3% of genes displayed a much more significant loss of NPM1c binding and, importantly, more pronounced gene expression reduction with dTAG-13 treatment (Fig. 1H and I). These data show the NPM1c's spreading into the gene body marks a set of highly expressed genes that is directly regulated by NPM1c. This link between oncoprotein binding and gene expression has previously been validated in the transcriptional regulation by MLL-fusion oncoprotein (28). We further evaluated the distribution of Pol II as well as the transcription regulators Menin (Menin–MLL complex) and ENL (SEC) at the genes with gene body spreading. We found all three components displaying strong signals across the gene body of the highly expressed genes marked by NPM1c gene body spreading (Supplementary Fig. S2C).

In our NPM1c binding analysis, we also observed NPM1c binding to active enhancer regions in both the OCI-AML3 cell line and AML-5583 blasts (Supplementary Fig. S2D).

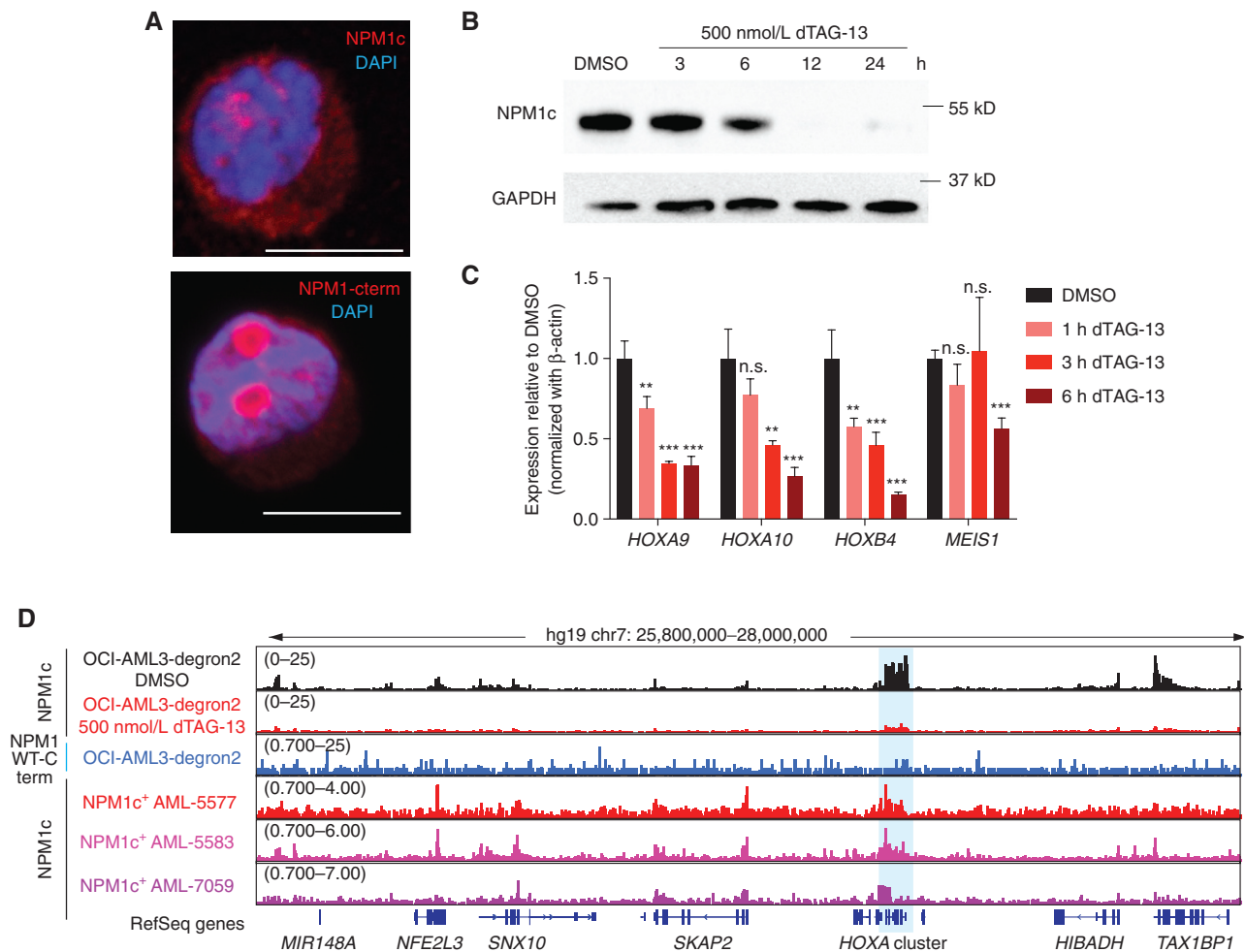


Figure 1. NPM1c binds to active promoter regions genome-wide. **A**, Immunostaining of NPM1c and NPM1-WT (c term) of OCI-AML3 cells. Scale bar = 10 μ m. **B**, Time-dependent degradation of NPM1c-FKBP12 fusion protein with 500 nmol/L dTAG-13 in the OCI-AML3 NPM1c degran 2 cell line. DAPI was used to stain DNA in the nucleus. **C**, Expression of *HOXA9*, *HOXA10*, *HOXB4*, and *MEIS1* after the 500 nmol/L dTAG-13 treatment for the indicated time. Mean \pm SEM is shown. $n = 3$. P value was calculated with a pairwise t test (DMSO vs. treatment). n.s., not significant; **, $P < 0.01$; ***, $P < 0.001$. **D**, The Integrative Genomics Viewer view of NPM1c and NPM1-WT CUT&RUN data in OCI-AML3 NPM1c degran 2 cells treated with DMSO or 500 nmol/L dTAG-13 for 24 hours and three primary NPM1c⁺ AML blasts of different comutation profiles. The *HOXA* cluster and the surrounding regions are shown. Reads per genomic bin (10 bp) were used to normalize the aligned reads. The mutation profile of NPM1c⁺ AML is as follows: AML-5577: *IDH1*^{R132H}, NPM1^{W288fs}, insertion CCTG. AML-5583: *DNMT3A*^{R882H}, *FLT3*-ITD; NPM1^{W288fs}, insertion TCTG. AML-7059: *TET2*^{mut}; *CEBPA*^{mut}; NPM1^{W288fs}. (continued on next page)

Particularly, certain NPM1c peaks in these enhancer regions disappeared after the degradation of NPM1c (Supplementary Fig. S2D and S2E), suggesting NPM1c may also play a role in active enhancers. An additional binding motif analysis revealed NPM1c-bound enhancer regions were enriched for myeloid transcriptional factor binding, suggesting a potential function of NPM1c at myeloid-specific enhancers (Supplementary Fig. S2F). Further, we identified several novel targets including differentiation-blocking Iroquois Homeobox transcriptional factors *IRX3* and *IRX5* (Fig. 1J and K; Supplementary Fig. S2G; ref. 29). Both genes were downregulated upon dTAG-13 degradation of NPM1c within a short time (Fig. 1J and K; Supplementary Fig. S2G). Importantly, high *IRX3* and *IRX5* expression correlates strongly with *NPM1* mutation status in The Cancer Genome Atlas AML patient cohort (Supplementary Fig. S2H and S2I).

NPM1c Maintains Active Transcription at Its Target Loci

As we observed a rapid loss of gene expression upon depletion (Fig. 1C), we speculated that NPM1c directly maintains the active transcription of its target genes. We performed CUT&RUN for NPM1c, Pol II, and known transcriptional regulators of *HOXA* genes—Menin and the SEC subunit ENL—following NPM1c degradation in OCI-AML3 NPM1c degran 2 cells (Fig. 2A). Under the DMSO-treated control condition, NPM1c, Pol II, Menin, and ENL displayed very similar binding profiles with peaks at the transcriptional start sites (TSS) of NPM1c-bound genes ($n = 6,312$; Supplementary Fig. S3A). We observed a time-dependent loss of NPM1c, Pol II, Menin, and ENL at NPM1c target genes upon dTAG-13 treatment (Fig. 2B–G). Next, we performed an Pol II elongation analysis with Pol II CUT&RUN data. We observed a global increase in the Pol II pausing index at 6 hours of dTAG-13 treatment

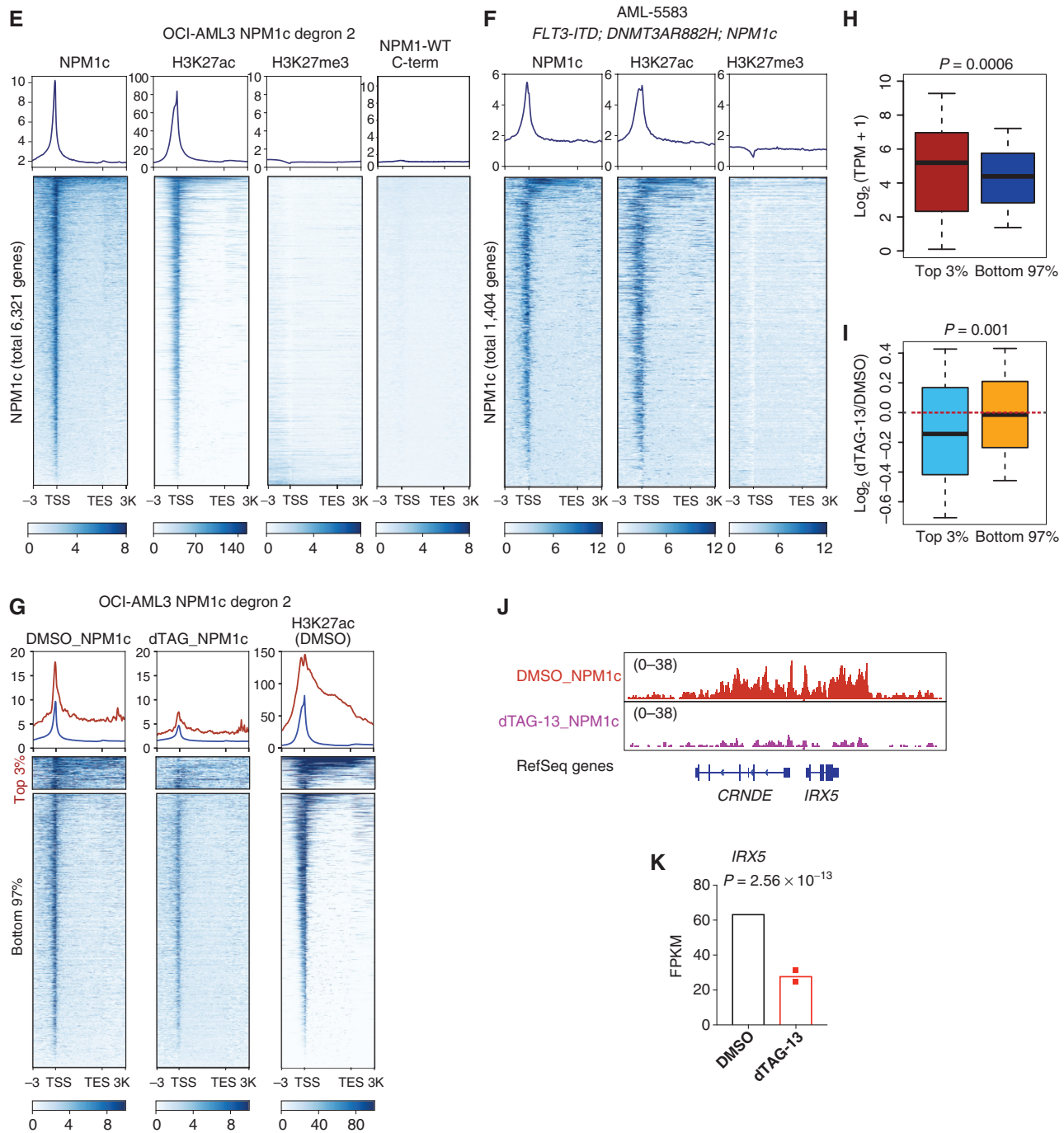


Figure 1. (Continued) **E** and **F**, The binding profiles of NPM1c, H3K27ac, and H3K27me3 at 6,312 NPM1c binding genes (**E**; OCI-AML3 NPM1c degran 2 cells) and 1,404 NPM1c genes (**F**; NPM1c⁺ AML-5583 blasts). TES, transcriptional end site. **G**, The metaplot of NPM1c binding profile of top 3% of genes and bottom 97% of NPM1c binding genes in OCI-AML3 NPM1c degran 2 cells under DMSO and 500 nmol/L dTAG-13 treatment. The metaplot of H3K27ac of the top 3% and bottom 97% NPM1c binding genes is also shown. **H**, Expression of the top 3% and bottom 97% NPM1c target genes. P value is calculated by the Wilcoxon rank test. Median, 25th percentile, and 75th percentile are plotted for the middle, top, and bottom box lines. Whisker indicates the maximum and minimum values in the data. TPM, transcripts per kilobase million. **I**, Expression fold change of top 3% and bottom 97% NPM1c target genes in 500 nmol/L dTAG-13-treated cells in comparison with DMSO-treated cells. P value is calculated by the Wilcoxon rank test. Median, 25th percentile, and 75th percentile are plotted for the middle, top, and bottom box lines. Whisker indicates the maximum and minimum values in the data. **J** and **K**, NPM1c's binding profile at *IRX5* locus (**J**) and expression value (FPKM) of *IRX5* (**K**) with 24 hours of 500 nmol/L dTAG-13 treatment. Mean \pm SD is shown. $n = 2$. P value is calculated by DESeq2. FPKM, fragments per kilobase million.

and a further increase when the treatment was extended to 24 hours (Supplementary Fig. S3B–S3D), suggesting a defect in Pol II elongation upon NPM1c degradation. To further

validate this, we performed nascent RNA labeling (Bru-seq) to examine the direct impact on transcription upon NPM1c degradation. We found a significant loss of nascent

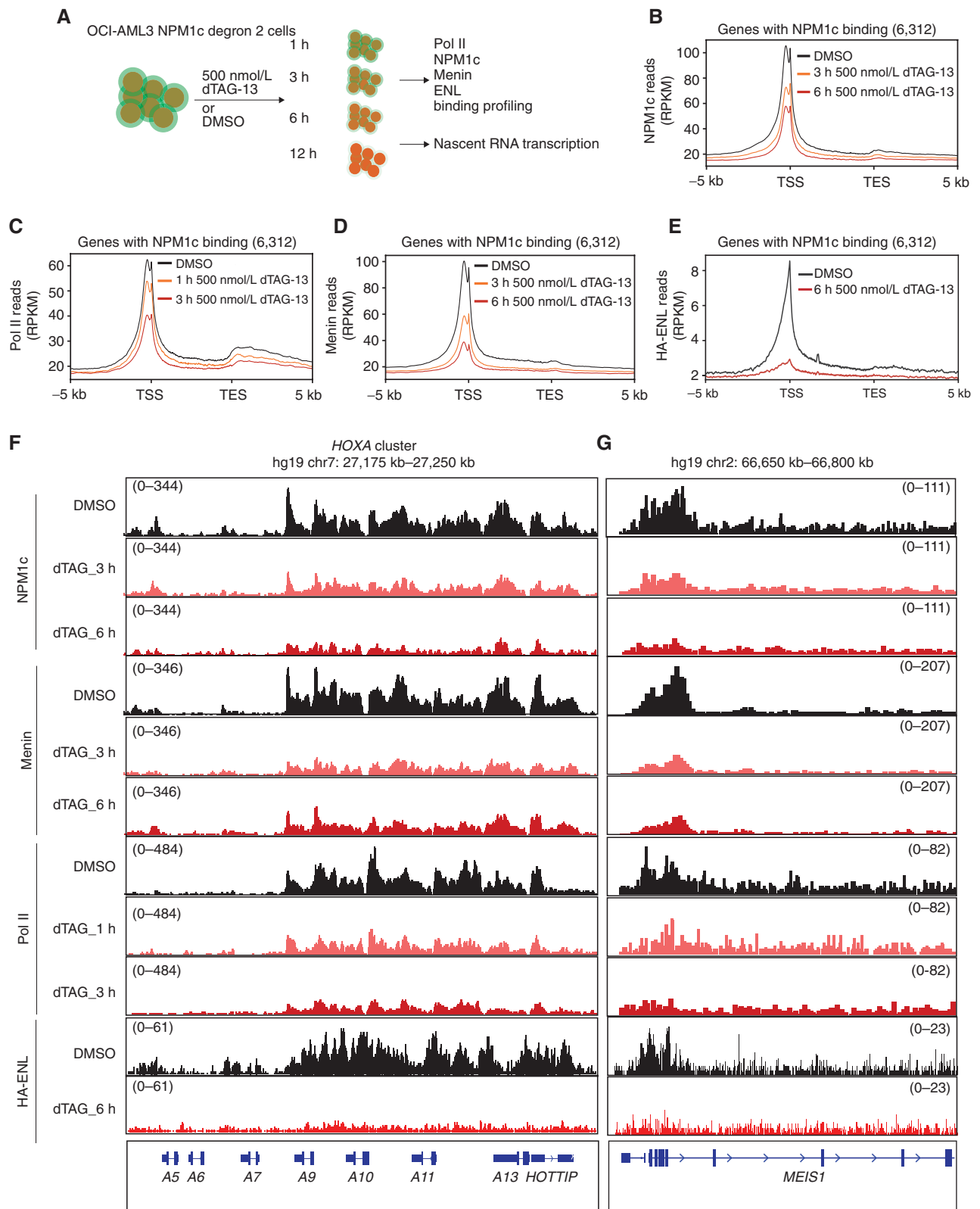


Figure 2. NPM1c directly modulates the transcription of leukemic genes via chromatin hijacking of Pol II and other transcriptional regulators. **A**, The experiment scheme of short time period NPM1c degradation. **B–E**, Normalized binding profiles of NPM1c (**B**), Pol II (**C**), Menin (**D**), and HA-ENL (**E**) on 6,312 NPM1c binding genes in OCI-AML3 NPM1c degron 2 cells treated with 500 nmol/L dTAG-13 for the indicated time. RPKM, reads per kilobase million; TES, transcriptional end site. **F** and **G**, The example Integrative Genomics Viewer view of NPM1c, Pol II, Menin, and HA-ENL enrichment at the *HOXA* cluster (**F**) and the *MEIS1* locus (**G**) with 500 nmol/L dTAG-13 treatment for the indicated time. (continued on next page)

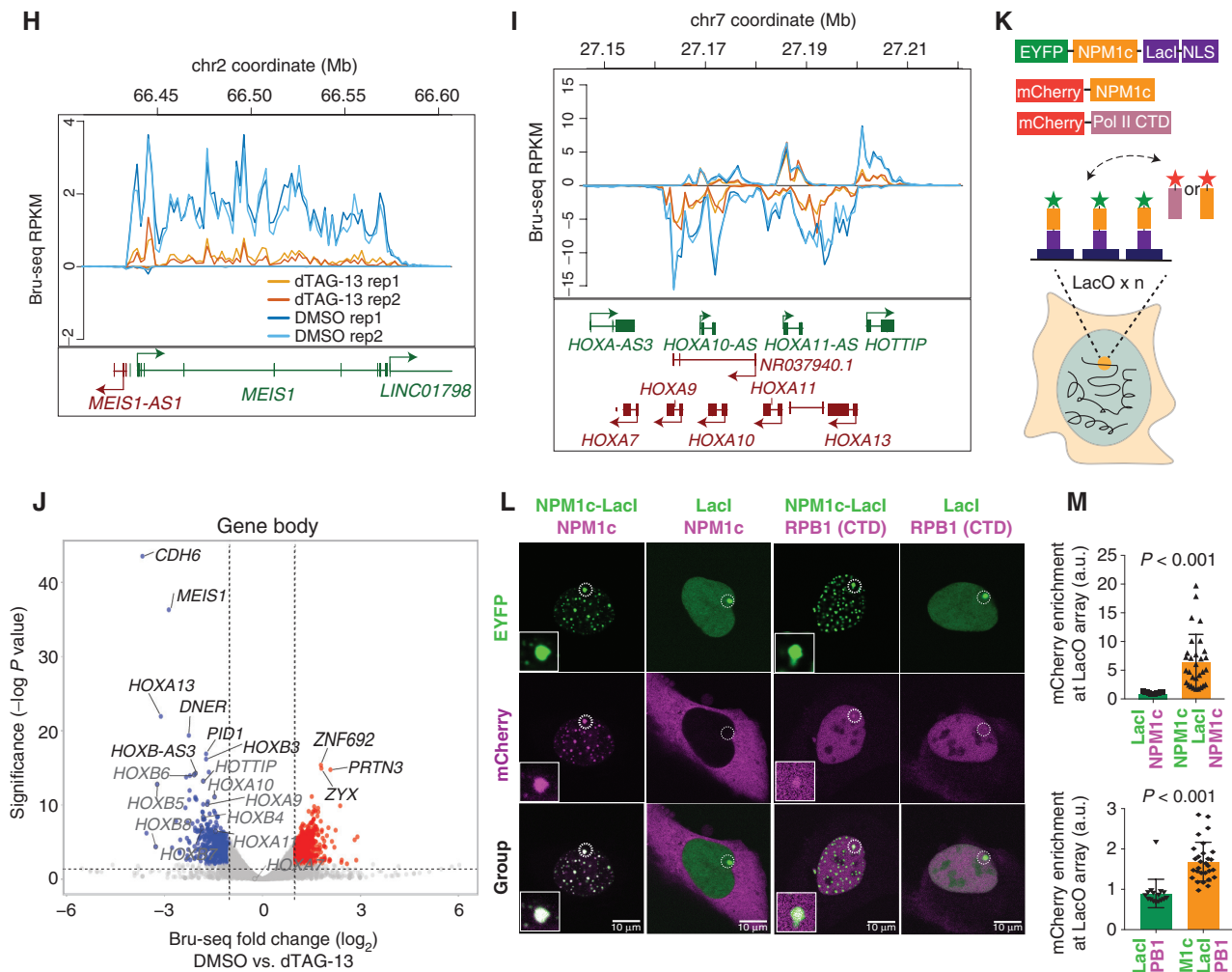


Figure 2. (Continued) **H** and **I**, Bru-seq track of the *HOXA* cluster (**H**) and *MEIS1* locus (**I**) of OCI-AML3 NPM1c degron 2 cells treated with DMSO or 500 nmol/L dTAG-13 for 12 hours. **J**, The volcano plot shows the differential transcription genes on the gene body Bru-seq reads with 12-hour treatment of OCI-AML3 NPM1c degron 2 cells with 500 nmol/L dTAG-13. The horizontal dashed line indicates the cutoff for $P = 0.01$. The vertical dashed line indicates the 1.5-fold cutoff for fold change in gene expression. **K**, The LacI-LacO array system to study the multivalent homotypic/heterotypic interactions between NPM1c and other transcription machinery protein on genomic loci. NPM1c-LacI is labeled with EYFP, and NPM1c or RPB1-CTD is labeled with mCherry. If heterotypic/homotypic interaction exists, both EYFP- and mCherry-labeled protein will form puncta at endogenous LacO array. NLS, nuclear localization signal. **L**, Two-color confocal fluorescence images of U2OS LacO array cell cotransfected with EYFP-LacI with NPM1c-mCherry or RPB1-CTD mCherry (left two columns), and images of cells cotransfected with EYFP-NPM1c-LacI with NPM1c-mCherry or RPB1-CTD mCherry (right two columns). The LacO array locus is circled, and magnified LacO array locus images are shown at the lower left part of the image. **M**, Enrichment of mCherry signal quantification at the LacO array locus in the cells transfected in **L**. Mean \pm SD is shown. P value is calculated by the Student t test.

transcription at the *HOXA/B* clusters and *MEIS1* genes, as well as a significant decrease in gene body transcription, showing a clear loss of transcriptional elongation at these NPM1c target loci (Fig. 2H-J; Supplementary Fig. S3E and S3F). Interestingly, Bru-seq revealed a global increase in the promoter-proximal reads and an increase in the pausing index, which is consistent with the Pol II CUT&RUN data (Supplementary Fig. S3G). We further tested the correlation between nascent RNA transcription change at promoter and gene body with the NPM1c binding change. We found that NPM1c binding changes at the gene body were highly correlated with gene body transcription change after NPM1c degradation (Supplementary Fig. S3H). This correlation is

even stronger at NPM1c gene body spreading genes (Supplementary Fig. S3I).

Next, we explored the mechanism by which NPM1c regulates the occupancy of transcriptional regulators and Pol II on chromatin. NPM1-WT contains an IDR and a C-terminal basic region with nucleoli localization signal (NoLS). Both regions have been shown to contribute to LLPS underlying the nucleolus formation through homotypic and heterotypic multivalent interactions (7, 30). The NPM1c frameshift mutations lead to the loss of the C-terminal aromatic NoLS but leave the other regions critical for multivalent interactions intact. This leads to the possibility that NPM1c retains the ability to form condensate through multivalent interactions.

We hypothesized that NPM1c could serve as a hub to stabilize other regulatory factors (Pol II, Menin, and ENL) binding to target genes through multivalent homotypic and heterotypic interactions. We used biotinylated isoxazole to allow for the formation of condensates that can be precipitated (Supplementary Fig. S4A). NPM1c were found in precipitated condensates as NPM1-WT (Supplementary Fig. S4A). Along with NPM1c, we observed the enrichment of Pol II and Menin in the precipitated condensates (Supplementary Fig. S4B). When similar experiments were performed with cells treated with dTAG-13, we found a loss of NPM1c as well as Pol II and Menin from the precipitation fraction (Supplementary Fig. S4C). To further test NPM1c's ability to form a transcriptional hub in living cells, we utilized the "LacO array assay," a cell imaging assay that detects IDR-mediated homotypic and heterotypic multivalent interactions at a synthetic array of LacO sequences incorporated in the U2OS genome, to measure NPM1c-mediated multivalent interactions on target genomic loci (Fig. 2K; refs. 31–33). We first expressed EYFP-tagged NPM1c-LacI fusion protein in the LacO-containing U2OS cells and observed its formation of numerous small-sized puncta in the nucleus (Supplementary Fig. S4D), suggesting strong homotypic interaction and LLPS propensity of NPM1c *in vivo*. We next expressed a second protein, mCherry-tagged NPM1c, in the cells and found it was significantly enriched at both the LacO array bound by EYFP-NPM1c-LacI and the self-assembled puncta of EYFP-NPM1c-LacI, confirming that NPM1c undergoes homotypic interactions (Fig. 2L). LacI does not contribute to the observed interactions, as NPM1c is not enriched at the LacO array bound by LacI only. Quantification of mCherry-NPM1c enrichment at the LacO array in the presence of EYFP-NPM1c-LacI versus EYFP-LacI is shown in Fig. 2M. Importantly, when the C-terminal domain (CTD) of the Pol II subunit RPB1 is coexpressed with EYFP-NPM1c-LacI, we clearly observed the recruitment of RPB1-CTD to the LacO array (Fig. 2L and M). Again, the LacI-only control did not recruit RPB1-CTD to the LacO array. These results together suggest that NPM1c functions as a scaffold protein to concentrate Pol II and other regulatory proteins such as Menin into high local concentration transcription hubs/condensates, thereby maintaining the active transcription state of target genes. We further tested the heterotypic interaction between NPM1c and NPM1-WT, and we found that NPM1-WT could be recruited to the LacO array, but not other small puncta of NPM1c. Vice versa, NPM1c could not be recruited to the NPM1-WT-marked nucleolus region (Supplementary Fig. S4E). These data suggest the heterotypic interactions between NPM1c and NPM1-WT are not as strong as homotypic interactions of NPM1c. Additionally, we did not observe a significant enrichment of ENL and Menin to the LacO array by NPM1c-LacI (Supplementary Fig. S4F). The data suggest that ENL's and Menin's initial recruitment to chromatin may depend on the active transcription given NPM1c's ability to form heterotypic interactions with Pol II CTD.

NPM1c Antagonize HDAC Activity to Maintain Active Chromatin State at Target Loci

To further explore NPM1c's modulation of active transcription, we performed a wash-off of dTAG-13 after 1 day

of treatment and evaluated whether NPM1c would return to chromatin and reactivate its target genes like a typical transcriptional factor (Fig. 3A). Time-course experiments showed that the global protein level of NPM1c returned to the basal level 4 days after wash-off (Fig. 3B). Remarkably, one day of dTAG-13 treatment was sufficient to trigger continuous differentiation of the OCI-AML3 NPM1c degran 2 cell line over a course of 4 days (Fig. 3C). Despite the recovery of NPM1c protein at day 4 after dTAG-13 wash-off, the expression of NPM1c canonical targets remained downregulated in the undifferentiated cells (Fig. 3D). Interestingly, at the chromatin level, although the global loss of NPM1c chromatin enrichment was not reversed 4 days after wash-off, NPM1c was found at its super-peak target loci (e.g., *HOXA*, *HOXB*, and *MEIS1*) at a similar enrichment level as in DMSO-treated cells (Fig. 3E; Supplementary Fig. S5A–S5D), suggesting a recovery of NPM1c binding preferentially at top target genes. However, the active histone mark H3K27ac decreased significantly after NPM1c degradation and did not return to the level of DMSO-treated cells 4 days after wash-off (Fig. 3E). This loss of H3K27ac mainly occurred at the differentially expressed NPM1c target genes, while other H3K27ac-marked regions did not show significant alteration following dTAG-13 treatment or wash-off (Supplementary Fig. S5E–S5G). These data strongly suggest that, besides maintaining active transcription, NPM1c also antagonizes the chromatin-modifying complex that silences the leukemic target loci. Due to the rapid loss of H3K27ac and the stable distribution of H3K27me3 during wash-off (Fig. 3E; Supplementary Fig. S5H), we hypothesized that the HDAC complex was actively involved in suppressing NPM1c target genes upon NPM1c depletion. To test this hypothesis, we cotreated the OCI-AML3 NPM1c degran 2 cell line with dTAG-13 and the pan-HDAC inhibitor vorinostat (SAHA; Fig. 3F). Treating the cells with SAHA alone increased *HOXA* gene expression. Meanwhile, cotreatment of SAHA and dTAG-13 reversed the downregulation of the *HOXA* cluster and *MEIS1* genes by dTAG-13 alone (Fig. 3G). Concomitantly, the continuous differentiation phenotype triggered by 1 day of dTAG-13 treatment was reversed by SAHA with the recovery of the H3K27ac signal at key NPM1c target sites (Fig. 3H and I). Next, we tested whether HDACs are recruited to chromatin after NPM1c degradation. We chose to test the chromatin binding of HDAC1, an essential subunit of the nucleosome remodeling and deacetylase (NuRD) complex, to study the HDACs' binding dynamics. Interestingly, we found that the occupancy of HDAC1 at NPM1c target sites was largely similar in DMSO- and dTAG-13-treated cells, suggesting that NPM1c antagonizes the function rather than chromatin binding of HDAC1 (Supplementary Fig. S5I and S5J). Finally, we observed that HDAC1 was bound to top NPM1c target genes such as the *HOXA* cluster (Supplementary Fig. S5K). These data support a model whereby HDACs are present at NPM1c target leukemic genes, but the activity of these deacetylases is kept in check by the presence of NPM1c. Disabling this epigenetic silencing mechanism of the *HOXA* cluster and *MEIS1* gene during myeloid differentiation hyperactivated a set of leukemia-driving genes to maintain the diseased state (Fig. 3J). Interestingly, we observed in the LacO array recruitment assay, NPM1c-LacI

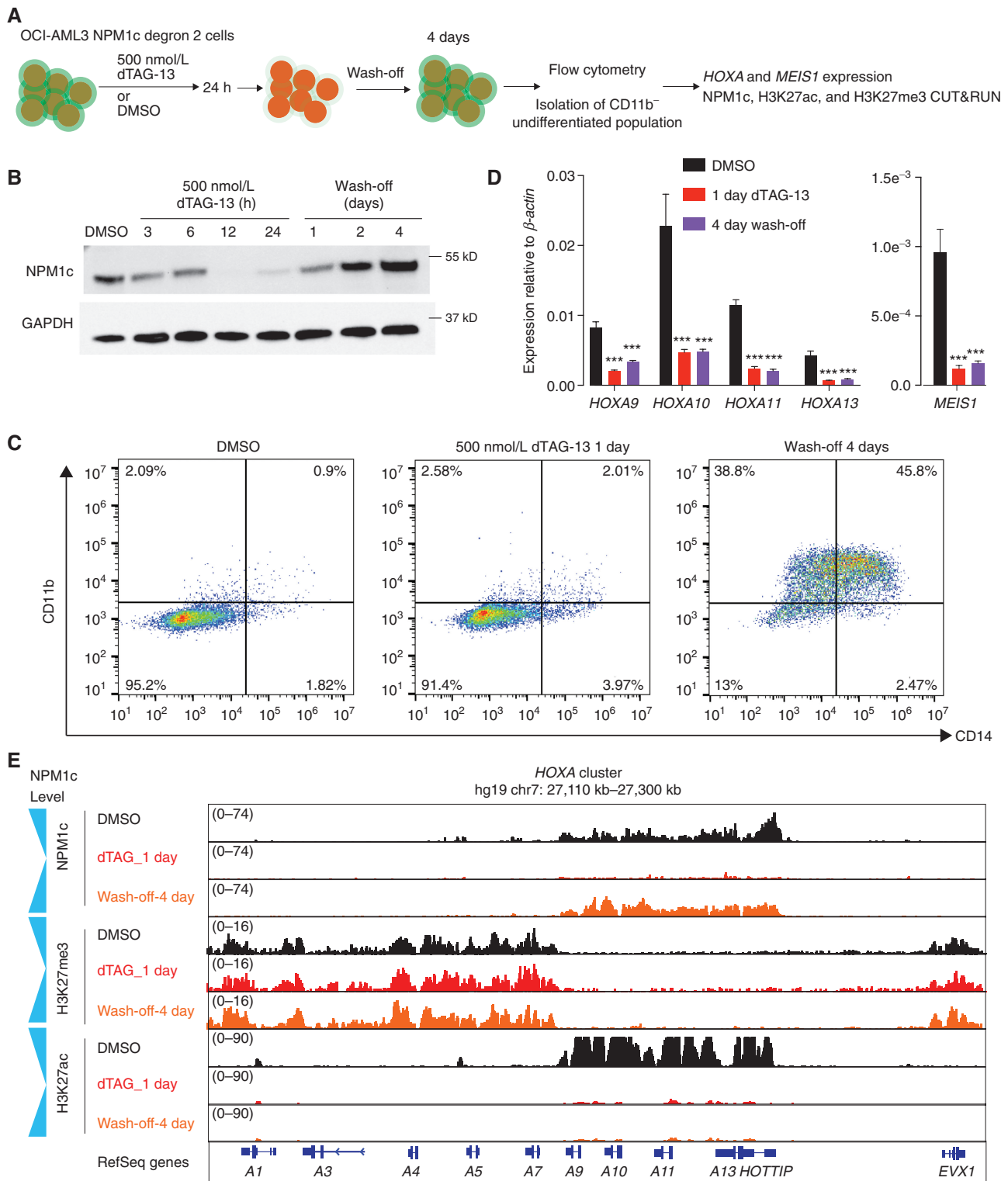


Figure 3. NPM1c maintains an active chromatin state by antagonizing HDAC activity. **A**, Experimental scheme of dTAG-13 wash-off experiments. **B**, The dynamic change of NPM1c-FKBP after the wash-off of dTAG-13 at days 1, 2, and 4 in OCI-AML3 NPM1c degran 2 cells. **C**, The dTAG-13-triggered continuous differentiation is measured by CD14 and CD11b flow cytometry. Representative flow cytometry plots are displayed. **D**, The expression of *HOXA* cluster genes and *MEIS1* in the cells after 1-day treatment with 500 nmol/L dTAG-13 and 4 days after dTAG-13 wash-off in OCI-AML3 NPM1c degran 2 cells. Mean \pm SD is shown. $n = 3$. Relative expression to β -actin is shown. P value is calculated by two-tail Student t test (DMSO vs. 1 day dTAG-13 and DMSO vs. 4 day dTAG-13 wash-off). ***, $P < 0.001$. **E**, Integrative Genomics Viewer view of NPM1c, H3K27me3, and H3K27ac binding profiles at the *HOXA* cluster after 1 day of dTAG-13 treatment and 4 days of dTAG-13 wash-off in OCI-AML3 NPM1c degran 2 cells. (continued on following page)

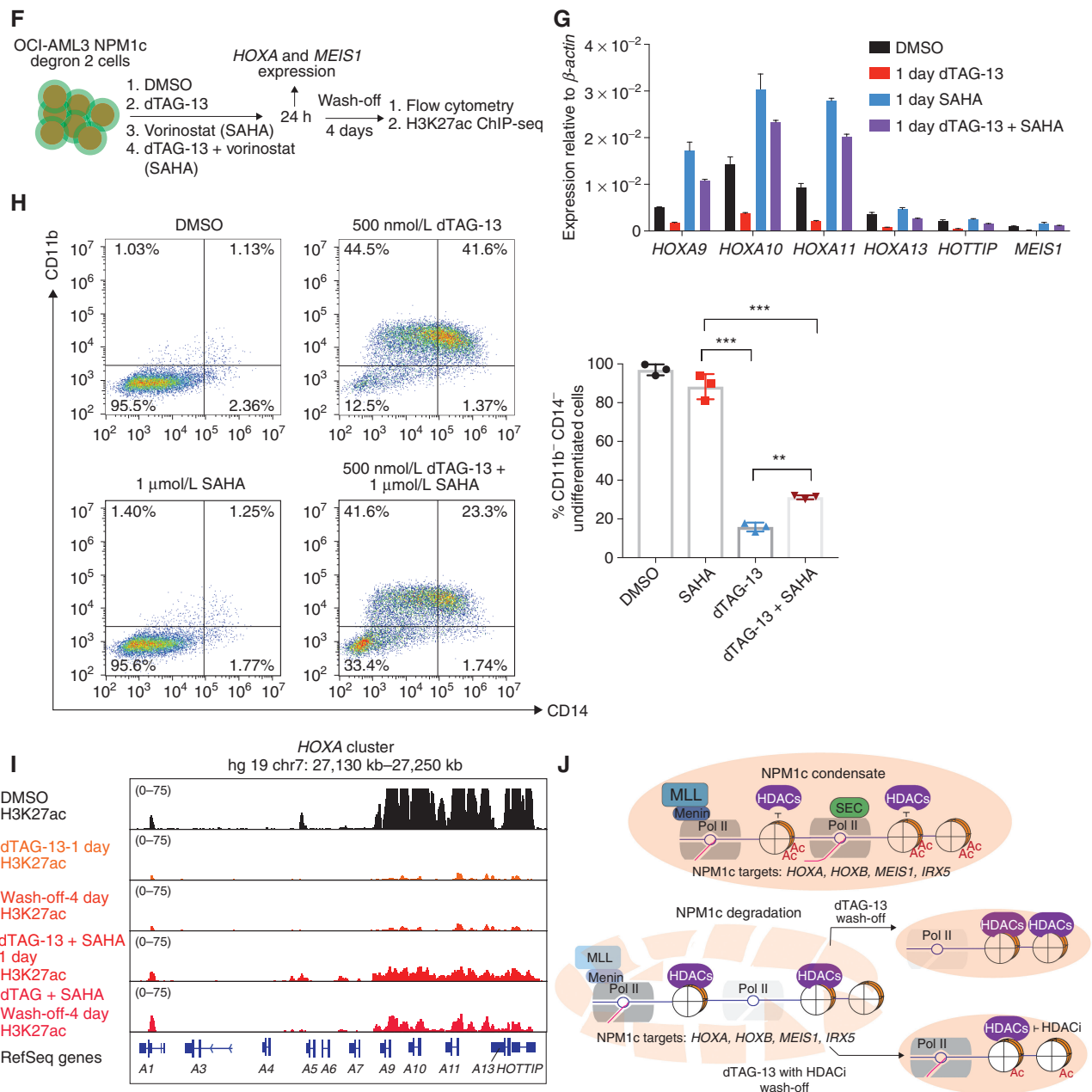


Figure 3. (Continued) **F**, Experimental scheme of dTAG-13 and HDAC inhibitor combination treatment experiments [dTAG-13, 500 nmol/L; vorinostat (SAHA), 1 μ mol/L]. ChIP-seq, chromatin immunoprecipitation and sequencing. **G**, Expression of *HOXA* genes and *MEIS1* in OCI-AML3 NPM1c degran 2 cells following 1-day treatments with DMSO, dTAG-13, SAHA, and dTAG-13 + SAHA. Mean \pm SD is shown. $n = 3$. Relative expression to β -actin is shown. **H**, Flow cytometry analysis with differentiation markers CD14 (x-axis) and CD11b (y-axis) of OCI-AML3 NPM1c degran 2 cells treated with DMSO, dTAG-13, SAHA, and dTAG-13 + SAHA for 1 day followed by 4 days of wash-off. Representative flow-cytometric plot is shown on the left. Quantification of undifferentiated CD11b⁺ CD14⁺ cells is shown on the right. $n = 3$; mean \pm SD is shown. P value is calculated by one-way ANOVA test with the Tukey test on all pairwise comparisons between treatment groups. **, $P < 0.01$; ***, $P < 0.001$. **I**, Integrative Genomics Viewer view of H3K27ac enrichment at the *HOXA* cluster in OCI-AML3 NPM1c degran 2 cells immediately after 1-day treatment and following 4-day wash-off of treatment with dTAG-13 or dTAG-13 + SAHA. **J**, Model of NPM1c's regulation of transcription and HDAC antagonism on chromatin for leukemic gene expression. NPM1c forms condensate to hijack the active transcription of target genes in AML—*HOXA/B* cluster genes, *MEIS1*, and *IRX5* (top). With degradation of NPM1c, Pol II and transcriptional complexes like SEC and MLL–Menin are displaced from NPM1c target genes. HDACs are activated and silence the chromatin state in NPM1c target genes (bottom left). With the wash-off of dTAG-13, continued differentiation is observed in cells after 24-hour pulse dTAG-13 treatment, with the silencing of NPM1c target genes initiated by HDACs (bottom right). Pulse vorinostat and dTAG-13 cotreatment leads to a significant delay of continued differentiation, with partial reversal of chromatin state and gene expression in comparison with dTAG-13 (bottom right). HDACi, HDAC inhibitor.

was able to recruit HDAC1 to the LacO array (Supplementary Fig. S5L and S5M). These data suggest that HDAC1 may also be present at NPM1c target loci from the initiation

of NPM1c AML. However, its function was antagonized by NPM1c at its target genes, possibly by active transcription hijacked by NPM1c.

NPM1c Hijacks and Amplifies Existing Active Transcription

In summary, our data reveal that NPM1c binds directly to chromatin and maintains the active transcription and chromatin state at target loci (Fig. 3J). This model also suggests that NPM1c acts by maintaining preexisting transcription rather than initiating transcription activation per se of its target genes. To test this notion, we performed a CRISPR-Cas9-mediated knockin of human NPM1c labeled with eGFP into a mouse bone marrow progenitor cell line immortalized by HOXB8 (Fig. 4A). The CRISPR-Cas9 knockin generated cells with endogenous labeling of NPM1c with GFP in heterozygous and homozygous fashion (Fig. 4B; Supplementary Fig. S6A and S6B). We clearly observed the cytoplasmic distribution of NPM1c-GFP by immunofluorescence and cell fractionation immunoblot (Fig. 4C; Supplementary Fig. S6A and S6B). RNA sequencing (RNA-seq) experiments identified 887 upregulated and 907 downregulated genes upon NPM1c knockin (Fig. 4D; Supplementary Table S3). We observed increased expression in genes involved in the p53 signaling pathway and decreased expression in genes involved in cell-cycle and homologous recombination pathways (Supplementary Fig. S6C and S6D). Of note, in the parental HOXB8 cells, key NPM1c targets identified in NPM1c⁺ leukemia cells (e.g., *HOXA/B*, *MEIS1*, and *IRX3/5*) were either not expressed or expressed at very low levels, and the expression of these genes was not induced by the introduction of NPM1c-GFP in this cell line (Fig. 4E). In contrast, several hematopoietic transcription factors expressed in the HOXB8 parental cell line (e.g., *Gata2*, *Hlf*, *Mycn*, and *Tal1*) were significantly overexpressed in the NPM1c-GFP clones (Fig. 4F). Next, we evaluated whether NPM1c was bound to chromatin in the HOXB8-transformed cell background. We found NPM1c significantly enriched at chromatin regions marked by active H3K27ac but devoid of the silencing H3K27me3 signal (Fig. 4G). Upon further scrutiny of the *Hoxa* locus, we found the entire cluster covered by strong H3K27me3 and without any noticeable binding of NPM1c (Fig. 4H). Similar strong enrichment of H3K27me3 was observed at the *Irx3* and *Irx5* genes (Supplementary Fig. S6E). Interestingly, the *Crnde* gene, located upstream of *Irx5*, showed enrichment of H3K27ac at its TSS, which was bound by NPM1c. Yet, this NPM1c binding did not induce the expression and chromatin status alteration of *Irx5*. Overall, these data show that NPM1c's targets are cell-type specific, and that NPM1c could not alter the chromatin state and initiate transcription activation. Additionally, we observed in mouse HOXB8 NPM1c-GFP cells a similar correlation between NPM1c gene body spreading and gene expression level as previously seen in OCI-AML3 cells (Supplementary Fig. S6F). The top 3% NPM1c binding genes in HOXB8 NPM1c-GFP cells showed significantly higher H3K27ac than the other 97% and also displayed stronger H3K27ac penetration into the gene body (Supplementary Fig. S6F). Importantly, the genes with NPM1c gene body spreading were more upregulated in HOXB8 NPM1c-GFP cells in comparison with HOXB8-WT cells (Supplementary Fig. S6G).

Next, we checked the gene expression and chromatin state of upregulated hematopoietic transcription factors in NPM1c-GFP clones (Fig. 4F). These transcription factors all have high basal expression levels in HOXB8 parental cells and

NPM1c clearly bound at their promoters and known hematopoietic enhancer upstream (*Gata2* -77 enhancer; Fig. 4I and J; Supplementary Fig. S6H and S6I; refs. 34-36). Furthermore, among all 1,224 genes with a significant upregulation trend upon NPM1c introduction, most were expressed in the parental cell line and marked with high levels of H3K27ac (Fig. 4K and L). H3K27ac binding in the upregulated genes also displayed a pattern with more broad distribution across the TSS and gene body than downregulated genes (Fig. 4L). These data further support a role for NPM1c in promoting active transcription.

Together, these data show that NPM1c acts to reinforce and amplify preexisting transcription activity rather than initiate *de novo* gene activation. Such a process could happen in normal HSPCs to boost the expression of self-renewal genes like *HOXA9* and *MEIS1*, which are already actively transcribed in normal HSPCs.

NPM1c's Binding to Chromatin Requires XPO1's Preexisting Binding to Chromatin

Next, we investigated whether the binding of NPM1c to chromatin requires a partner. The nuclear export protein XPO1 has been shown to export NPM1c as its cargo (2, 22, 23), and recent studies have shown that XPO1 is capable of chromatin binding (22, 37). Therefore, we performed CUT&RUN of XPO1 in OCI-AML3 NPM1c degron 2 cells and found it bound to chromatin with striking overlap with NPM1c binding regions (Fig. 5A and B). This overlap was also observed in primary AML blasts and the NPM1c-GFP HOXB8 mouse bone marrow progenitor cell line (Supplementary Fig. S7A-S7D). Further immunoprecipitation of nuclear protein from OCI-AML3 cells showed NPM1c and XPO1 interacting with each other and forming protein complexes mediated by NES (Fig. 5C). Immunofluorescence imaging showed the colocalization of the two proteins inside the nucleus (Fig. 5D). Interestingly, we found that both XPO1 and NPM1c formed puncta structures in the nucleus, many of which were colocalized at the nuclear periphery. Next, we wondered whether inhibition of XPO1's nuclear export function could alter the chromatin enrichment of XPO1 and NPM1c. To avoid the nonspecific XPO1 degradation effect, we used a relatively low concentration of the XPO1 inhibitor selinexor that has been shown to be sufficient to relocate NPM1c from cytosol to the nucleus (16, 23). To our surprise, despite the retention of NPM1c to within the nucleus upon XPO1 inhibition, we observed a significant loss of chromatin enrichment of both NPM1c and XPO1 (Fig. 5E-G). In contrast, degradation of NPM1c by dTAG-13 treatment only resulted in a significant loss of NPM1c but not XPO1 chromatin enrichment at the 6,312 NPM1c target genes (Fig. 5E-G). These data indicate that NPM1c is not required for XPO1's chromatin binding in NPM1c⁺ AML cells.

Further, we could observe a significant overlap between genes downregulated in both dTAG-13 and selinexor treatment in the OCI-AML3 NPM1c degron 2 cell line (Fig. 5H; Supplementary Table S4). These genes were enriched for canonical leukemic targets of NPM1c and displayed loss of nascent transcription at their gene body (Fig. 5I and J). This further supports a model where XPO1 and NPM1c form a

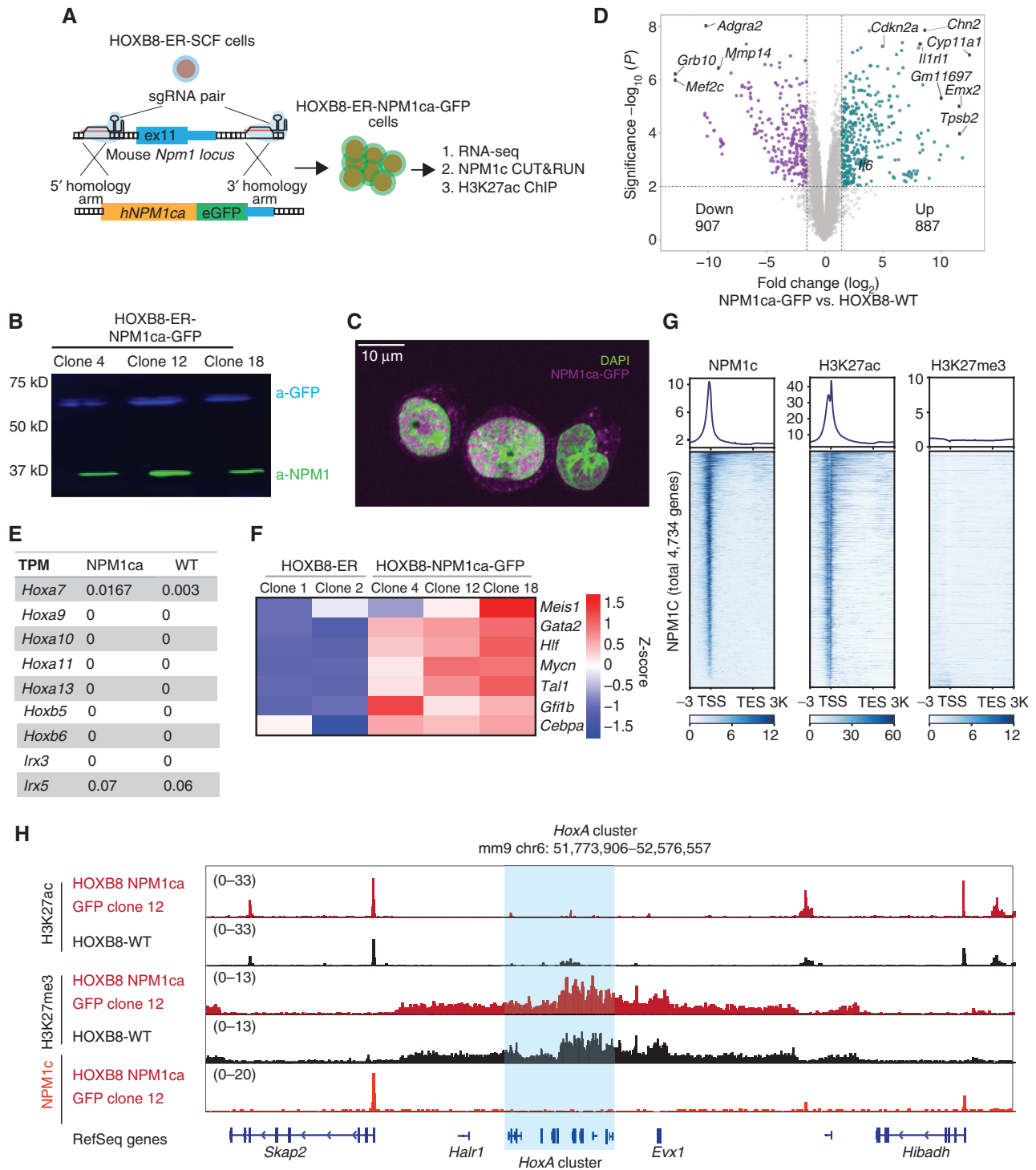


Figure 4. NPM1c's hijacking of active transcription is cell-type specific and depends on cell type-specific chromatin state. **A**, The scheme of CRISPR-Cas9 HDR-mediated knockin of human NPM1ca-eGFP (NPM1c type A) in a mouse HOXB8-ER-immortalized cell line. The CRISPR knockin results in the replacement of exon 11 and 3' UTR of mouse *Npm1* genes to human NPM1c exon with eGFP and 3' UTR of mouse *Npm1* gene. ChIP, chromatin immunoprecipitation; sgRNA, single-guide RNA. **B**, Two-color Western blot showing the presence of both NPM1ca-GFP and NPM1-WT in HOXB8 NPM1ca-eGFP cell line clones 4, 12, and 18. **C**, Confocal image of NPM1ca-eGFP clone 12 on the cytoplasm and nuclear localization of NPM1ca-eGFP. Scale bar = 10 μ m. **D**, Volcano plot showing the differentially expressed genes in NPM1ca-GFP clones vs. parental HOXB8-ER cell lines. The horizontal dashed line indicates the cutoff for $P = 0.01$. The vertical dashed line indicates the 1.5-fold cutoff for fold change. **E**, Table of mean transcripts per kilobase million (TPM) value of *HoxA/B* cluster genes as well as *Irx3* and *Irx5* in NPM1ca clones ($n = 3$) and HOXB8-ER parental cell lines ($n = 2$). **F**, Heat map of Z-score of differentially expressed hematopoietic transcriptional factors. **G**, The NPM1c, H3K27ac, and H3K27me3 binding profiles on genes with NPM1ca binding ($n = 4,734$) in NPM1ca clone 12 cells. TES, transcriptional end site. **H**, Integrative Genomics Viewer view of NPM1c, H3K27ac, and H3K27me3 enrichment and distribution at the *HoxA* cluster of NPM1ca clone 12 and HOXB8-ER parental cell lines. The blue shaded area indicates the *HoxA* cluster from *Hoxa1* to *Hottip*. (continued on next page)

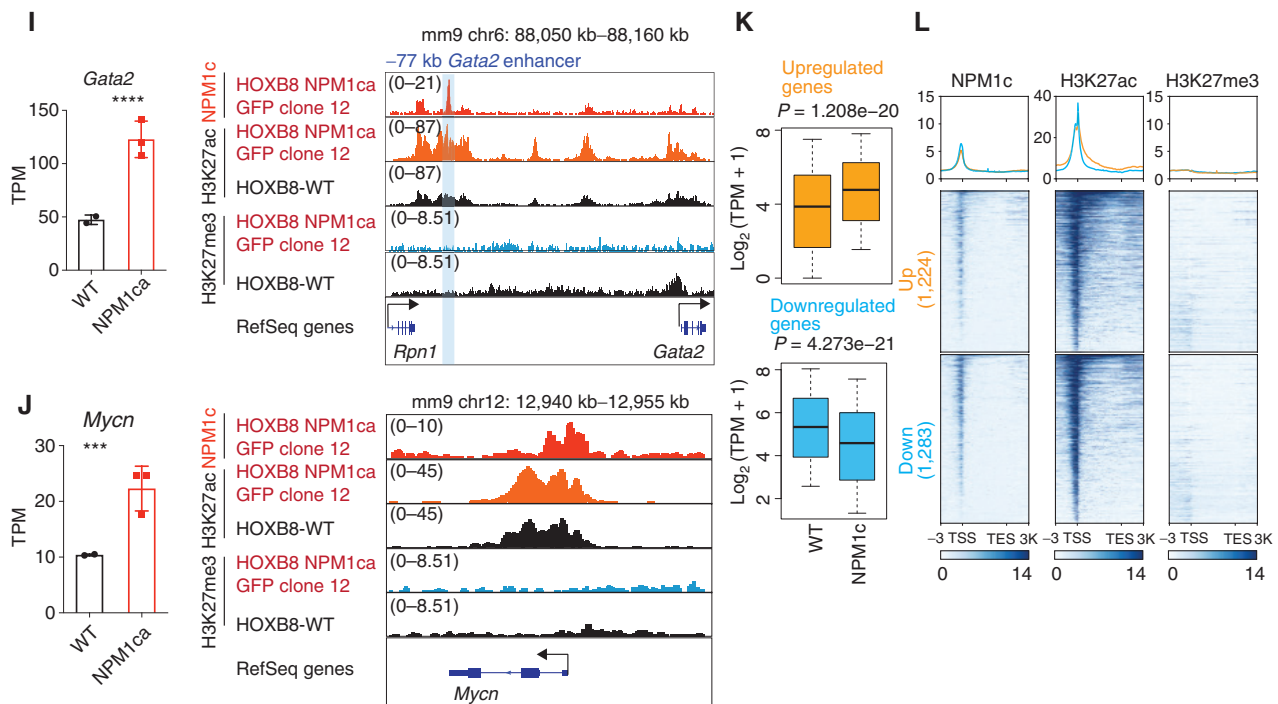


Figure 4. (Continued) I and J, Left, gene expression alteration of *Gata2* (I) and *Mycn* (J). Right, NPM1c, H3K27ac, and H3K27me3 enrichment and distribution at the *Gata2* (I) and *Mycn* (J) locus in the NPM1c clone 12 cell and HOXB8-ER parental cell line. The blue shaded area indicates the -77 enhancer of *Gata2* previously reported (35–37). Mean \pm SD is shown in the TPM plot. $n = 3$ for NPM1c group. $n = 2$ for the WT (HOXB8-ER parental cell line) group. **K**, Box plots showing the expression level of upregulated and downregulated genes. Median, 25th percentile, and 75th percentile are plotted for the middle, top, and bottom box lines. Whisker indicates the maximum and minimum value in the data. **L**, The binding profiles of NPM1c, H3K27ac, and H3K27me3 in genes upregulated and downregulated in NPM1c clones compared with parental HOXB8-ER in **K**. The NPM1c profile plots the CUT&RUN data of NPM1c from NPM1c-GFP clone 12 cells. H3K27ac and H3K27me3 profiles plot the CUT&RUN data from the parental HOXB8-ER cell line. A heatmap showing TPM of the corresponding genes in NPM1c-GFP clones and the parental HOXB8-ER cell line is shown on the right. Upregulated genes and downregulated genes are filtered only by $P < 0.05$. The gene expression fold change was omitted.

complex to promote active transcription at leukemic targets. We tested the interaction between NPM1c and XPO1 by using LacI-LacO array assay, and we found NPM1c-LacI could recruit XPO1 to LacO and other NPM1c-LacI puncta in the nucleus (Fig. 5K and L). These data suggest that NPM1c may also enhance XPO1's binding to chromatin. To further elucidate the chromatin binding dependency between these proteins, we next performed CUT&RUN of XPO1 in both Kasumi-1 and MOLM-13 leukemia cell lines, which feature AML1-ETO and MLL-AF9 fusions, respectively, as well as CD34⁺ HSPCs, all lacking NPM1c mutations. We observed XPO1 clearly bound to early transcriptional factors like *RUNX1* and *MEIS1* loci in the leukemia cell lines, but there was no indication of chromatin enrichment in HSPCs (Supplementary Fig. S7E–S7G). These results indicated that XPO1 chromatin enrichment is not dependent on the presence of NPM1c, but can be enhanced by the presence of the mutated protein.

Although NPM1c's chromatin binding requires interaction with XPO1, XPO1 itself appears capable of chromatin binding by itself or through interaction with other yet undiscovered cofactors. Nevertheless, the introduction of NPM1c seems to provide a “feed-forward” mechanism whereby both proteins reinforce each other and hijack actively transcribed genes, including those responsible for HSPC self-renewal. This, in turn, could lead to the initial leukemia

development phase with the NPM1c hijacking of preexisting chromatin-bound XPO1.

XPO1 and Menin Inhibitors Displayed Synergy in NPM1c AML

Menin inhibitors have shown a promising effect on NPM1c⁺ AML in recent preclinical studies and early clinical trials (11, 38, 39). Multiple XPO1 inhibitors (selinexor and eltanexor) have also been approved as drugs or are actively being tested in clinical trials for multiple hematopoietic malignancies (40, 41). Here, we tested whether the XPO1 inhibitors and Menin inhibitors could show synergy against NPM1c⁺ AML. We chose to study the XPO1 inhibitor eltanexor for its better pharmacodynamic and pharmacokinetic properties over selinexor (42). We found that the combination of eltanexor and the Menin inhibitor MI-3454 synergistically reduced the expression of *HOXA/B* cluster genes, *MEIS1*, and *FTL3* and promoted cell differentiation (Fig. 6A; Supplementary Fig. S8A and S8B). We next performed a drug synergy assay on the effect of cell growth with OCI-AML3 and other non-NPM1c hematopoietic malignancy cell lines. We found that eltanexor and MI-3454 mainly showed an additive effect on cell growth (Bliss score less than 10; Supplementary Fig. S8C–S8G). However, the two compounds have a synergistic effect in reducing the undifferentiated cells (Fig. 6B; Supplementary Fig. S8H and

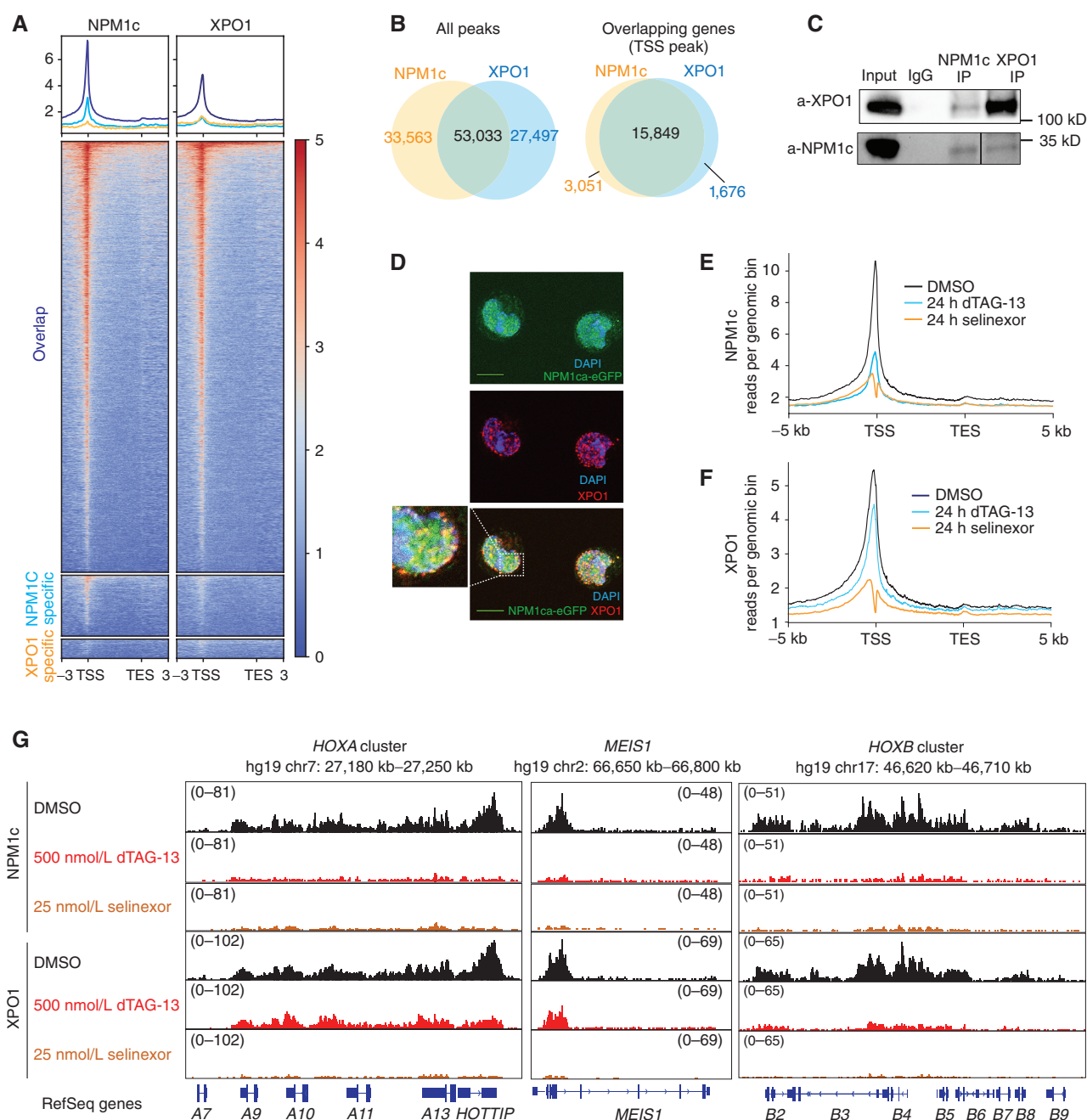


Figure 5. XPO1 nuclear export inhibition displaces NPM1c from chromatin. **A**, The binding profiles of NPM1c, XPO1, and H3K27ac at NPM1c binding genes in OCI-AML3 cells from -3 kb TSS to $+3$ kb transcriptional end site (TES). **B**, The peak overlap between NPM1c and XPO1 peaks (left) and genes with TSS peak (right) in OCI-AML3 NPM1c degnon 2 cells. **C**, Coimmunoprecipitation (IP) of NPM1c and XPO1 in OCI-AML3 cells. **D**, Confocal immunofluorescence image of colocalization of NPM1c-eGFP and XPO1 in NPM1c-eGFP HOXB8 cells. DAPI was used to stain the DNA of the nucleus. Scale bar = $10 \mu\text{m}$. **E** and **F**, The NPM1c (**E**) and XPO1 (**F**) binding profiles in 6,312 NPM1c binding genes with 500 nmol/L dTAG-13 and 25 nmol/L selinexor treatment for 24 hours in OCI-AML3 NPM1c degnon 2 cells (-5 kb TSS to $+5$ kb TES). **G**, Integrative Genomics Viewer view of NPM1c and XPO1 enrichment and distribution at the *HOXA* cluster, *MEIS1*, and the *HOXB* cluster in OCI-AML3 NPM1c degnon 2 cells with 500 nmol/L dTAG-13 and 25 nmol/L selinexor treatment. (continued on next page)

S8I). In particular, we found that short-term treatment with eltanexor was sufficient to maintain long-term differentiation with MI-3454, suggesting a treatment scheme that can avoid the toxicity of nuclear export inhibitors (Supplementary Fig. S8J). We then tested Menin-XPO1 combination inhibition with primary AML blasts with an *in vitro*

colony formation assay and patient-derived xenograft (PDX) mouse model. We found a synergistic effect in reducing the colony number of NPM1c⁺ AML blasts but no such effect in non-NPM1c AML (Fig. 6C; Supplementary Fig. S8K). We could also validate that the eltanexor concentration does not affect the colony formation ability of normal CD34⁺ HSPCs

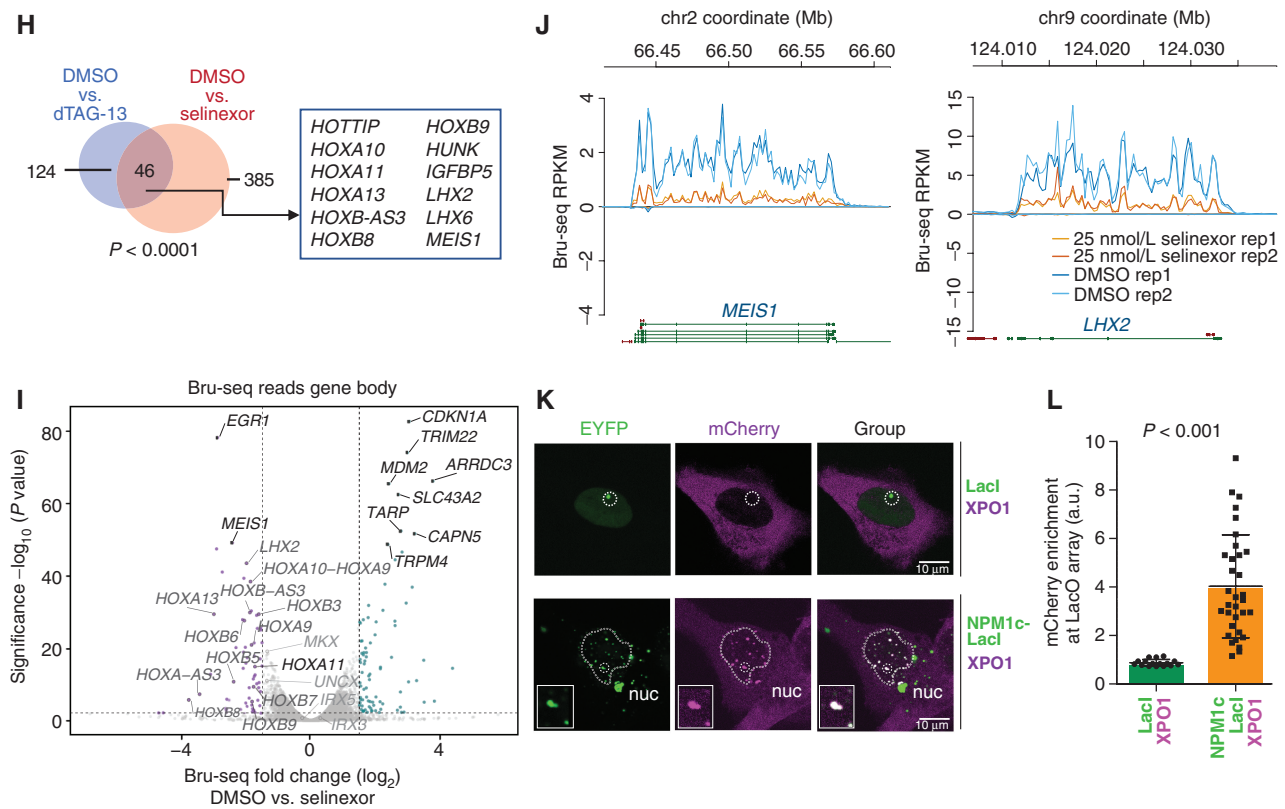


Figure 5. (Continued) **H**, Venn diagram showing the overlap between the downregulated genes in dTAG-13 and selinexor treatment. The representative overlapping genes are listed. P value is calculated by the Fisher exact test for 2×2 contingency table. **I**, The volcano plot shows the differential transcription genes on the gene body Bru-seq reads with 12 hours of 25 nmol/L selinexor treatment in OCI-AML3 NPM1c degran 2 cells. The horizontal dashed line indicates the cutoff for $P = 0.01$. The vertical dashed line indicates the 1.5-fold cutoff for fold change in gene expression. **J**, The Bru-seq reads of nascent transcription at the *MEIS1* (left) and *LHX2* (right) locus. RPKM, reads per kilobase million. **K**, Two color confocal fluorescence images of a U2OS LacO array cell cotransfected with EYFP-LacI with mCherry-XPO1 (top), and images of cells cotransfected with EYFP-NPM1c-LacI and mCherry-XPO1 (bottom). The LacO array locus is circled, and magnified LacO array locus images are shown at the lower left part of the image. The nucleus (nuc) is annotated in the bottom images. **L**, Enrichment of mCherry signal quantification at the LacO array locus in the cells transfected in **K**. Mean \pm SD is shown. P value is calculated by the Student t test.

(Supplementary Fig. S8L). Importantly, we performed the leukemia burden assay with the PDX model of NPM1c⁺ AML and found the two compounds together showed more durable effects than either compound by itself in reducing the human AML engraftment without significant toxicity in reducing body weight (Fig. 6D; Supplementary Fig. S8M).

DISCUSSION

Overall, our data show an unexpected function of NPM1c as a direct transcription amplifier for several leukemic transcription factors including the *HOXA/B* cluster genes and *MEIS1*. Thus, NPM1c is a neomorphic oncoprotein that maintains the active transcription of key leukemic genes involved in cellular self-renewal, which are also actively transcribed in normal HSPCs. NPM1c hijacks the transcription of these genes and prevents their silencing by HDACs during myeloid differentiation, thereby blocking the differentiation program of the cell of origin in NPM1c⁺ AML (Fig. 6E and F). During normal myeloid differentiation, the silencing process of *HOXA/B* cluster genes and *MEIS1* is likely initiated by the myeloid lineage-specific repressing transcriptional factors (like GFI1). Such repressing transcriptional factors then

recruit HDACs as corepressors to silence *HOXA/B* cluster genes and *MEIS1* to allow the proper myeloid differentiation (43). This neomorphic regulatory function of NPM1c likely depends on the heterotypic interactions between NPM1c and other regulators, including SEC and Menin.

The frameshift mutation to NPM1c disables a C-terminal nucleolus localization signal and introduces a novel NES. Given the cytoplasmic enrichment of NPM1c, a role in transcription regulation by NPM1c seems counterintuitive. Yet, the mutated protein still retains two nuclear localization signals (NLS), enabling it to actively shuttle between the nucleus and cytoplasm (2, 3, 6). This feature makes NPM1c capable of regulating transcription directly through multivalent homotypic and heterotypic interactions during its transit in the nucleus with adequate concentration. Additionally, we have observed a significant decrease in the size of condensate formed by NPM1c in comparison with NPM1-WT, which marks the nucleolus. This decrease in the condensate size also suggests that NPM1c could form a transcriptional hub with the transcription complex like Pol II—other than forming mesoscale phase separation puncta that exclude transcriptional complex and chromatin protein (44–46). Given that NPM1c in the nucleus has to be at the right concentration

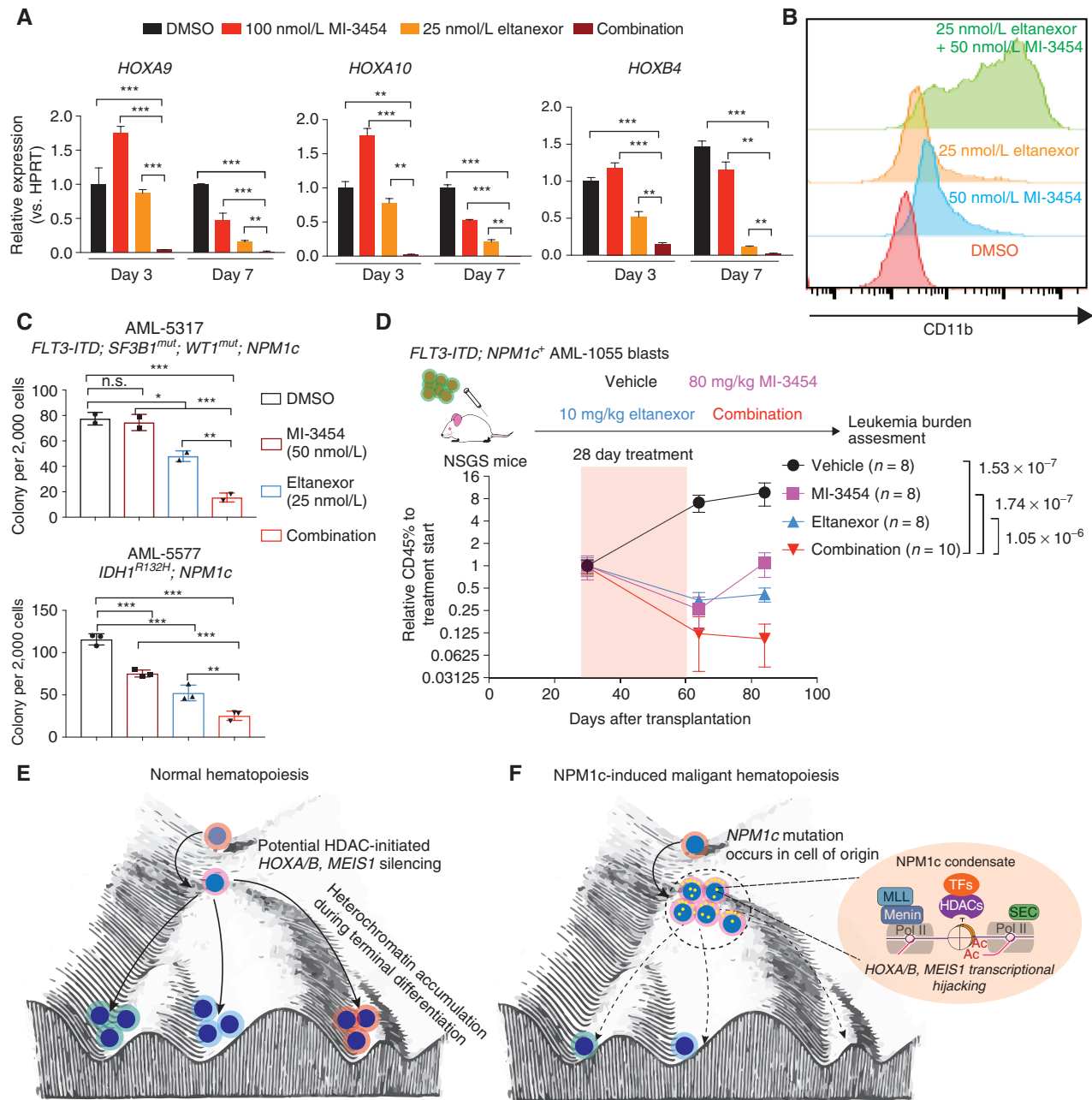


Figure 6. XPO1 inhibition synergizes with Menin inhibitor in NPM1c leukemia treatment. **A**, *HOXA9*, *HOXA10*, and *HOXB4* relative expression levels after treatment with 50 nmol/L MI-3454, 25 nmol/L eltanexor, and combination of the two in OCI-AML3 cells. $n = 3$; mean \pm SEM is shown. P value is calculated by one-way ANOVA test with Tukey test on all pairwise comparisons between treatment groups. *, $P < 0.05$; **, $P < 0.01$; ***, $P < 0.001$. **B**, Differentiation (CD11b flow cytometry) induced by 7-day treatment with 50 nmol/L MI-3454, 25 nmol/L eltanexor, and combination of the two in OCI-AML3 cells. **C**, *In vitro* colony-forming assay of NPM1c AML blasts with DMSO, 50 nmol/L MI3454, 25 nmol/L eltanexor, and the combination. $n = 3$; mean \pm SD is shown. P value is calculated by one-way ANOVA test with Tukey test on all pairwise comparison between treatment groups. $n = 2$ for AML-5317. $n = 3$ for AML-5577. n.s., not significant; *, $P < 0.05$; **, $P < 0.01$; ***, $P < 0.001$. **D**, Leukemia burden assay scheme with NSGS mice (left). Leukemia burden after vehicle, MI-3454, eltanexor, and combination treatment (right). Mean \pm SD is shown. The number of mice in each group is listed. P value is calculated by t test of hCD45 engraftment at day 84 after transplantation comparing between the combination group and all other groups. **E**, The normal differentiation process in hematopoiesis. During the normal hematopoiesis process, the *HOXA/B* cluster and *MEIS1* are stepwise silenced through chromatin modification. First, in the HSPCs ready to differentiate, active histone acetylation marks will be removed by HDACs. Then during terminal differentiation, heterochromatin marks like H3K27me3 will accumulate in the *HOXA/B* cluster and *MEIS1* to fully silence the *HOXA/B* cluster and *MEIS1*. This will ensure the proper shutdown of stem cell self-renewal genes and prevent the ectopic expression of the *HOXA/B* cluster and *MEIS1*. **F**, When NPM1c mutation occurs in the leukemia cell of origin (likely HSPCs), the NPM1c protein will form multicomponent condensate through multivalent heterotypic interactions. This formation of condensate will lead to transcriptional amplification of the *HOXA/B* cluster and *MEIS1* genes and prevent the initial step during normal hematopoiesis to silence the gene by HDACs. This transcriptional hijacking by NPM1c will not only lead to the arrest of gene expression at the HSPC stage but also block the differentiation initiated by HDACs. TF, transcription factor.

to act as a transcriptional amplifier, cytoplasmic NPM1c not only provides a reservoir for NPM1c to enter the nucleus but also prevents the excessive accumulation of NPM1c in the nucleus and the formation of chromatin-exclusive LLPS puncta.

Our data did not exclude the possibility that repressors of the *HOXA* cluster/*MEIS1* are sequestered by NPM1c in the cytoplasm (16, 19). However, based on our and others' data, such a loss of repression is not the initiating event for *HOXA/B* cluster gene activation. Additionally, our data clearly show that there is no global loss of silent genomic mark in NPM1c⁺ AMLs and there is no immediate Polycomb repression at the *HOXA* cluster after NPM1c degradation (Fig. 3E; Supplementary Fig. S5H). These data together suggest that the potential heterochromatin repression may accumulate much later after the NPM1c degradation.

Together, our data suggest NPM1c's hijacking of direct transcription is the most plausible mechanism for NPM1c's activation of leukemic genes like *HOXA9* and *MEIS1* in leukemia development. NPM1c also involves several other processes in the cytoplasm. These functions of NPM1c likely involve RNA binding and processing, which are known functions of NPM1-WT. In addition, our data show that XPO1 clearly binds to chromatin in leukemia cells with various mutation backgrounds. Such interaction is not a canonical function of the nuclear export protein and is sensitive to nuclear export inhibitors in NPM1c⁺ AML. Interestingly, our data and previously published works show that the XPO1 binding to chromatin is cell-type specific and displays very different genomic enrichment in mouse embryonic stem cells and leukemia, but not normal CD34⁺ HSPCs (22, 38). These data suggest, as a protein without genuine DNA or chromatin binding motif, XPO1's chromatin binding may depend on its interacting RNA or protein cargo. XPO1's accumulation on chromatin revealed a novel aspect of the biological function of the protein, which can be targeted by XPO1 inhibitors. We also revealed that XPO1 and Menin inhibitors used in combination displayed synergistic effects that can be exploited as a therapeutic strategy to treat NPM1c⁺ AML. Given both compounds are currently in clinical trials, a combination therapy can potentially be brought to a clinical setting rapidly to achieve more controlled toxicity or better outcome for NPM1c⁺ AML patients.

Our proposed model is limited to explaining leukemogenesis in which NPM1c is involved. During leukemogenesis, mutations in *NPM1* are always among the second wave of events that accelerate toward the leukemia state. NPM1c⁺ leukemias are often initiated by earlier comutations during the preleukemia incubation (11, 47). Therefore, it is highly likely that the earlier mutations preprogram the chromatin landscape and transcriptomics for NPM1c to hijack. Such mechanisms may include the step-wise recruitment of XPO1 to chromatin by the early mutations in clonal hematopoiesis, as we do not observe the binding of XPO1 in normal human CD34⁺ HSPCs. The early mutation to key genes such as *DNMT3A*, *TET2*, and *IDH1/2* may lead to the binding of XPO1 to chromatin with altered regulatory RNA production. Alternatively, *NPM1c* mutations co-occur with cell signaling mutations like *FLT3-ITD* mutation. Interestingly, *FLT3-ITD* mutations would significantly accelerate the leukemogenesis

process initiated by NPM1c (48, 49). Such acceleration may indicate that the additional general cell proliferation chromatin landscape changes enhance the chromatin state and transcriptional changes induced by NPM1c alone (48). Given the nature of long-term evolution and cellular heterogeneity in the transcriptomic and epigenomic data from the NPM1c AML mouse model, future single-cell analyses will better dissect the early molecular events induced by NPM1c alone. A more tailored NPM1c mouse model would also be required to further dissect these changes.

METHODS

Cell Lines and Primary Human AML Samples

The OCI-AML3-NPM1c-FKBP12-T2A-GFP degon cell line (OCI-AML3 NPM1c degon 2) was a gift from Dr. Margaret Goodell (Baylor College of Medicine). WT OCI-AML3 cells were obtained from DSMZ. MOLM13, H929, SEM, and MV4:11 cells were obtained from Jolanta Grembecka's lab (originally from DSMZ and ATCC). HOXB8-SCF cells were a gift from Dr. David Sykes from Massachusetts General Hospital. Cell lines were verified free from *Mycoplasma* infection every 2 months using PCR detection. Cell lines were thawed and used to perform experiments within a 7- to 10-passage period.

Cell lines were verified with HiC for copy-number variation, and the OCI-AML3-NPM1c-FKBP12-T2A-GFP degon cell line was further checked with expression of GFP, Sanger sequencing, and immunoblot to verify the expression of NPM1c-FKBP12 fusion protein. Primary human AML samples were purchased from the Stem Cell and Xenograft Core at the University of Pennsylvania from deidentified frozen mononuclear cells from patients with AML. Samples were selected for the *NPM1* w288fs mutation status. Samples were obtained after IRB consent and provided to us as annotated, anonymous samples. Mononuclear cells were thawed by directly pipetting ice-cold PBS + 2% BSA to frozen cells in the freezing vials at room temperature. Thawed mononuclear cells were then gradient-separated with Lymphoprep (StemCell Tech). Buffy coat was then collected to enrich the living cells.

CRISPR-Cas9 Knockin of NPM1c-GFP in the HOXB8 Cells

CRISPR-Cas9-mediated NPM1c-GFP knockin was performed as previously described. Single-guide RNAs were obtained by using a HiScribe T7 High Yield RNA Synthesis Kit (NEB) or ordered directly from Synthego. RNP complex is assembled by using 2 μ g Cas9 (IDT), 1 μ g guide RNA targeting the last intron of *Npm1*, 1 μ g guide RNA targeting the 3' UTR region of *Npm1*, and 1 μ g HDR dsDNA template. The detailed oligo sequences are listed in Supplementary Table S5. GFP⁺ cells were sorted by FACS and genotyped for the integration of NPM1c-GFP.

CUT&RUN and RNase CUT&RUN

CUT&RUN and RNase CUT&RUN were performed with nuclear extraction. Basically, 0.5 to 2 \times 10⁶ fresh cells were harvested and extracted for the nucleus using nuclear extraction buffer (20 mmol/L HEPES pH 7.9, 0.5 mmol/L spermidine, 10 mmol/L KCl, 0.1% Triton-X, 20% glycerol with protease inhibitor) on ice for 5 to 10 minutes. In the XPO1 CUT&RUN performed with MOLM13 cells and CD34⁺ HSPCs, cells were fixed 1% formaldehyde for 1 minute. Then fixation was stopped with 125 mmol/L glycine for 5 minutes. Cell pellets were collected and then proceeded to the nuclear extraction step described above.

After washing with Wash Buffer 2 (20 mmol/L HEPES pH 7.5, 0.5 mmol/L Spermidine, 0.1% BSA, 150 mmol/L NaCl with protease inhibitor), nuclei were incubated with activated Concanavalin A Beads (Bang Labs) for 10 minutes at room temperature. Nuclei were

then washed and incubated with antibodies at 4°C with 35 rpm rotation for 2 hours (H3K4me3, H3K27ac, H3K27me3, Menin, XPO1), 4 hours (NPM1c, NPM1-WT), or overnight (Pol II). pA/G MNase (Epiccypher) or pA-MNase (gift from Dr. Steve Henikoff, Fred Hutchinson Cancer Center) were then incubated with the nuclei-bead mixture in wash buffer 2 at 4°C with 35 rpm rotation for 1 hour. After washing with Wash Buffer 2 for two times, CaCl₂ was added to nuclei to activate the MNase to release chromatin. Stop buffer (340 mmol/L NaCl, 20 mmol/L EDTA, pH 8.0, 4 mmol/L EGTA, 50 µg/mL RNase A, 50 µg/mL glycogen) was added to stop the MNase, and digestion of chromatin was performed with 5 µL proteinase K at 55°C overnight. DNA was extracted using phenol:chloroform:isoamyl alcohol (Sigma) extraction and a MaXtract high-density tube (Qiagen). The aqueous phase was taken, and DNA was precipitated with 1/10 volume of 3M Sodium Acetate, pH 5.2, and 2.5 volume of 100% ethanol at -20°C overnight. DNA was precipitated by 30 minutes of centrifugation at 4°C and washed with 70% cold ethanol. Libraries were made using the Swift Bioscience Acce-NGS 2G plus kit according to the manufacturer's manual. The library was sequenced 150-bp paired-end on HiSeq 3000 by Fulgent Genomics.

RNase CUT&RUN was performed following the protocol described before with modification (26). Basically, nuclei were extracted and digested with or without RNase at room temperature for 90 minutes. RNase-treated nuclei then proceeded to the steps above for bead binding, antibody incubation, pA/G MNase incubation, and DNA isolation. Libraries were prepared using the Swift Bioscience Acce-NGS 2G plus kit according to the manufacturer's manual. Libraries were sequenced by Fulgent rent-a-lane service with the HiSeq platform. The reads were aligned to the hg19 genome with the Bowtie 2 software with the following parameters as previously described: bowtie2 -x -doovetail -phred33. The aligned reads were then filtered out of the PCR duplicates by Picard, and bamCoverage was used to generate the reads per genomic content (RPGC)– or reads per kilobase million (RPKM)–normalized bigwig track file with a bin size of 10 bp for visualization in Integrated Genome Viewer (IGV).

For the alignment to CHM13-T2T, bigwig files were visualized using the WashU epigenome browser in the CHM13-T2T option. bamCoverage was used to generate the RPGC-normalized bigwig track file with a bin size of 10 bp.

The antibodies used in CUT&RUN were as follows: NPM1c (Novus Biologicals, Rabbit Polyclonal, NB110-61,646, RRID:AB_964800), NPM1-WT (Novus Biologicals, Mouse Monoclonal, C-terminal, NB600-1030, RRID:AB_10001674), XPO1 (Novus Biologicals, Rabbit Polyclonal, NB100-79802, RRID:AB_2215823), Menin (Bethyl Lab, Rabbit Polyclonal, A300-105A, RRID:AB_2143306), Pol II (Diagenode, Mouse Monoclonal, C15200004, RRID:AB_2728744), H3K27ac (Diagenode, Rabbit Polyclonal, C15410196, RRID:AB_2637079), H3K4me3 (Cell Signaling Technology, Rabbit Monoclonal, 9751, RRID:AB_2616028), and H3K27me3 (Cell Signaling Technology, Rabbit Monoclonal, 9733, RRID:AB_2616029).

Peak Calling of NPM1c CUT&RUN Data

Quality control for the alignment of BAM files was performed by samtools (50), allowing only uniquely mapped reads to be retained, and then PCR duplicates were removed by Picard (<http://broadinstitute.github.io/picard/>) using the MarkDuplicates tool with the parameters "VALIDATION_STRINGENCY = LENIENT REMOVE_DUPLICATES = true" for downstream analyses. Significant NPM1 and CRM1 peaks calling was performed by MACS2 (51) callpeak command with default parameters except with "-q 0.05 -nolambda -broad -broad-cutoff 0.05." The peaks were then filtered by the length of ≥500 bp and the hg19 ENCODE blacklist (<https://www.encodeproject.org/files/ENCF001TDO/>). Statistically significant differential elements were identified using MAnorm (52), which normalizes read density levels and produces *P* values using MA plot

methods. Regions with an absolute *M* value of >1 and a *P* value of <0.01 were considered as gained or lost regions.

dTAG-13 Treatment

dTAG-13 (500 nmol/L–1 µmol/L; R&D Systems, 6605/5) was added to culture media with the indicated duration described in the text. Wash-off in Fig. 3 was performed after 1 day of dTAG-13 treatment by washing cells with PBS twice. Washed cells were taken out to assay for NPM1c degradation by Western blot. Protein was extracted using 2 × 10⁶ cells with NP40 lysis buffer. Antibodies used in the Western blots of Fig. 1 and Fig. 3 were NPM1c (Novus Biologicals, Rabbit Polyclonal, NB110-61646, RRID:AB_964800) and GAPDH (Cell Signaling Technology, Rabbit Monoclonal, #5174, RRID:AB_10622025).

Chromatin Immunoprecipitation Sequencing

Chromatin immunoprecipitation was performed using a previously described protocol (53). Briefly, 1 million cells were fixed with 1% formaldehyde and sonicated with Covaris E220 or Bioruptor Plus. Sonicated chromatin was then incubated with antibodies against target proteins or histone posttranslational modifications overnight. Protein A/G beads (Thermo Fisher) were added to the sonicated chromatin for 2 hours. After washes with low-salt, high-salt, and LiCl wash buffer, beads were decross-linked with proteinase K (Zymo Research) at 55°C overnight. Pulled-down DNA was extracted by the DNA clean and concentration kit (Zymo Research). Libraries were prepared using the Swift Bioscience Acce-NGS 2G plus kit according to the manufacturer's manual. The libraries were sequenced 150-bp paired-end on HiSeq 2000 by Fulgent Genomics.

Chromatin immunoprecipitation sequencing (ChIP-seq) antibodies used in this study included H3K27ac (Diagenode, Rabbit Polyclonal, C15410196, RRID:AB_2637079), H3K27me3 (Cell Signaling Technology, Rabbit Monoclonal, 9733, RRID:AB_2616029), Pol II S5P (Diagenode, Mouse Monoclonal, C15200007, RRID:AB_2713926), HDAC1 (Diagenode, Rabbit Polyclonal, C15410325, RRID:AB_2921266), anti-FLAG antibody (Sigma-Aldrich, mouse monoclonal, F1804, RRID:AB_262044), and anti-HA antibody (Abcam, Rabbit Polyclonal, ab9110, RRID:AB_307019).

mRNA-seq

mRNA-seq was performed as previously described (53). Total RNA from OCI-AML3 cells treated with DMSO, dTAG-13, and selinexor (ApexBio, B1464) with specific doses and time was isolated using the Qiagen RNeasy RNA isolation kit (micro). Sequencing libraries were prepared from 500 ng of total RNA using the NEBNext Poly(A) mRNA Magnetic Isolation kit and Swift Biosciences rapid RNA library kit following the manufacturer's protocol. Libraries were sequenced on the Illumina HiSeq 2000 platform at Fulgent Genetics to generate paired-end reads of 2 × 150 bp.

RNA-seq raw reads were mapped to the human genome (hg19) using STAR-2.6.1 (54) with default parameters. Transcript levels were calculated as transcripts per kilobase million (TPM) and counted using RSEM (55). Those genes having a count greater than 5 in at least 50% of the samples were kept for further examination. The DESeq2 R package was used to perform differential gene expression analysis between groups (56). Significantly differentially expressed genes were defined as those with a log₂ fold change value of >1 and a false discovery rate of <0.05.

Assay for Transposase-Accessible Chromatin Using Sequencing

Assay for Transposase-Accessible Chromatin using sequencing was performed with the Illumina Nextera XT library preparation kit (FC-131-1024, Illumina) as previously described (53). Upon 1-day

treatment with DMSO, 500 nmol/L dTAG-13, or 25 nmol/L selinexor, 50,000 OCI-AML3 NPM1c degnon 2 cells were harvested and permeabilized in 50 μ L of cold lysis buffer (10 mmol/L Tris-HCl, pH 7.4, 10 mmol/L NaCl, 3 mmol/L MgCl₂, 0.1% IGEPAL CA-630). The transposition reaction was carried out at 37°C for 30 minutes with agitation in 50 μ L volume containing 25 μ L of 2 \times TD buffer and 2.5 μ L of Nextera Tn5 transposase. DNA was purified with Qiagen MinElute PCR Purification Kit. Library amplification was done with the KAPA HiFi HotStart ReadyMix PCR kit, and the resulting libraries were purified with the Qiagen MinElute PCR Purification Kit. Libraries were sequenced in the Illumina HiSeq 2000 platform to generate paired-end reads of 2 \times 150 bp.

Paired-end reads were trimmed using Trim Galore (version 0.6.1) and aligned to hg19 using Burrows-Wheeler Aligner (bwa-mem, version 0.7.17). The resulting alignments were sorted, indexed using SAMtools (version 1.9), and marked for duplicates with sambalster (version 0.1.24). Reads were then normalized using deeptools bamCoverage with the RPGC and visualized with IGV.

Bru-seq

Bru-seq was performed with the previously described protocols (57). Briefly, 10⁷ OCI-AML3-NPM1c-FKBP12-T2A-GFP degnon cells were treated with DMSO, 500 nmol/L dTAG-13, or 25 nmol/L selinexor for 12 hours. Then, 5-BrUTP (Sigma, B7166) was added to the media to a concentration of 2 mmol/L. Thirty minutes later, cells were harvested after washing with PBS 2 times. Cells were then lysed in 1 mL TRIzol. The labeled RNA was extracted and proceeded to library construction in the University of Michigan Bru-seq core as previously described.

Sequenced reads were aligned to the hg19 genome using Bowtie2, the promoter-proximal and gene body reads were determined, and differential expression was called by NRSA v2.1 (58).

Chromatin Protein Salt Fractionation

Differential salt fraction of chromatin protein was performed based on the previous protocol (59) with minor modifications. First, 10⁷ OCI-AML3 NPM1c degnon 2 cells were lysed in hypotonic buffer (Nuclear Complex Co-IP Kit, Active Motif, 54001) on ice for 30 minutes to isolate cytoplasmic fraction. Nuclei were pelleted by centrifugation at 14,000 rpm for 5 minutes and were collected for MNase (NEB) digestion for 90 minutes at 4°C with rotation. Digested nuclei were centrifuged for 5 minutes at 600 \times g at 4°C, the supernatant was collected as MNase fraction, and the pellet was washed with MNase digestion buffer (10 mmol/L Tris, pH 7.4, 2 mmol/L MgCl₂, 0.1 mmol/L PMSF). Pellet was collected and digested with chromatin extraction buffer containing 80 mmol/L NaCl (10 mmol/L Tris, pH 7.4, 2 mmol/L MgCl₂, 2 mmol/L EGTA, 0.1% Triton X-100, 80 mmol/L NaCl) at 4°C with rotation for 30 minutes. Digested nuclei were centrifuged for 5 minutes at 600 \times g at 4°C, and supernatant was collected as an 80 mmol/L NaCl chromatin fraction. Pellet digestion and chromatin protein fraction collection were repeated with chromatin extraction buffer containing 150 mmol/L NaCl, 300 mmol/L NaCl, and 600 mmol/L NaCl.

LacO Array Imaging Assay

Human U2OS cells containing a LacO array with ~50,000 LacO elements in the genome were grown in low-glucose DMEM (Thermo Fisher, 10567014) with 10% fetal bovine serum (HyClone FBS SH30910.03) and 1% penicillin-streptomycin (Thermo Fisher, 15140122; ref. 32). For imaging sample preparation, cells were plated on 70% ethanol-pretreated, 18-mm circular micro cover glasses (No. 1, Electron Microscopy Sciences, 72229-01) on 12-well TC Treated Plates (Genesee, 25-106MP) and were transfected with the target constructs using Invitrogen Lipofectamine 3000 Transfection Reagent

(Thermo Scientific, L3000015) for 24 hours, followed by fixation with 4% paraformaldehyde (Sigma-Aldrich, P6148-500G) for 15 minutes. The pcDNA3.1-EYFP-NPM1c-LacI-SV40NLS expression vector was directly synthesized by GeneUniversal. cDNA of ENL (gift from Liling Wan), Menin (Addgene plasmid # 32079; RRID:Addgene_32079), HDAC1 (Addgene plasmid # 13820; RRID:Addgene_13820), and Pol II CTD (gift from Shasha Chong) were cloned into the pCMV-mCherry vector (gift from Shasha Chong) using the NEBuilder HiFi DNA Assembly kit (NEB, E2621S). The mCherry-XPO1 fusion protein expression vector was created by inserting the mCherry fragment into the pcDNA3.1-XPO1 ORF vector (NM_003400.4, GeneScript, cat. # OHu13444).

Fluorescence images were acquired on a Zeiss LSM 980 laser scanning confocal microscope operated by the Biological Imaging Facility of the Beckman Institute at Caltech, using a 63 \times , NA 1.4 Plan-Apochromat objective. Pinhole size was set to 1.00 AU, as the resolution was set to 512 \times 512 with a digital zoom of 3.0 \times and line averaging of 2. Excitation laser sources and emission ranges were 514 nm/508–561 nm (EYFP λ_{max} = 513 nm, λ_{em} = 530 nm, shown as green) and 594 nm/561–693 nm (mCherry λ_{max} = 587 nm, λ_{em} = 610 nm, shown as magenta). Each image was collected as a 3D stack of 25 to 40 images with a spacing of 0.24 μ m in the z-direction between slices. Before acquiring the two-color fluorescence images, we carefully tuned the emission filters to make sure no bleed-through existed between the two channels, and adjusted laser intensity and microscope detector gains to ensure that no pixel in the images was saturated.

We quantified protein-protein interactions from the two-color images in the following steps. First, we selected the slice (#N) in the EYFP channel z stack where a LacO-associated punctum had the highest fluorescence intensity, located the central pixel of the LacO array, and obtained the radial profiles of fluorescence intensity centering the pixel in both EYFP and mCherry channels. Second, we extracted the EYFP intensity radial profile and estimated the radius of the punctum as the distance from the central pixel at which the derivative of fluorescence intensity to distance first drops to zero. Next, we measured the maximum and peripheral mCherry intensities of the punctum. To average out the intensity noise at the single-pixel level, convolution was applied to image slice #N of the mCherry channel using a 5 \times 5 convolution kernel J_5 (all-ones matrix). Intensities of four convoluted pixels surrounding the peak intensity pixel were averaged as I_{peak} . Two values on the mCherry intensity radial profile at locations immediately outside the punctum periphery were averaged as $I_{\text{periphery}}$. Finally, we calculated the intensity ratio $I_{\text{peak}}/I_{\text{periphery}}$ as a measure of the mCherry enrichment at the LacO array. A ratio above 1 suggests protein-protein interactions.

Immunofluorescence and Structural Illumination Microscopy

Immunofluorescence was performed as described before (53). The cells were first fixed with 4% paraformaldehyde at room temperature for 15 minutes and were then permeabilized with PBS plus 0.1% Triton-X for 10 minutes at room temperature. Cells were then blocked by incubation with PBS plus 0.1% Tween-20 and 1% BSA for 30 minutes. First and secondary antibody incubation was performed at 4°C overnight and room temperature for 1 hour, respectively. Imaging was performed using Nikon A1 plus confocal microscopy. Multicolor image was processed and presented by ImageJ software.

For Structural Illumination microscopy, cells were stained with the same procedure. Anti-rabbit VHH Nanobody [Alpaca anti-Rabbit IgG Nano (VHH) Recombinant Secondary Antibody, Alexa Fluor 568, Thermo Fisher, SA5-10325, RRID:AB_2868372] was used for secondary antibody staining. Pictures were taken by NIKON N-SIM + A1R. The SIM image was built by NIS-Elements, and the size of NPM1c puncta and NPM1-WT marked nucleoli was measured by ImageJ “Analyze Particle” function.

Antibodies used in immunofluorescence were NPM1c (Novus Biologicals, Rabbit Polyclonal, NB110-61646, RRID:AB_964800), NPM1-WT (Novus Biologicals, Mouse Monoclonal, C-terminal, NB600-1030, RRID:AB_10001674), and XPO1 (Novus Biologicals, Rabbit Polyclonal, NB100-79802, RRID:AB_2215823).

Bio-Isoxazole Protein Precipitation

The OCI-AML3 NPM1c-degron 2 cell line was cultured to 10 million for each replicate. Then cells were treated with DMSO or 500 nmol/L dTAG-13 for 24 hours. Cells were extracted with 0.1% NP-40 buffer (50 mmol/L HEPES-NaOH, pH 7.4, 150 mmol/L NaCl, 1 mmol/L EDTA, 2.5 mmol/L EGTA, 10% glycerol, 1× protease inhibitor, 50 mmol/L NaF, 1 mmol/L DTT, 0.1% NP40; Thermo Fisher) for 30 minutes at 4°C with rotation as previously described (60). The cell extract was centrifuged at 16,600 × *g* for 15 minutes at 4°C. The supernatant was collected with 50 μL as input. Bio-Isoxazole (Sigma) was added to the remaining supernatant to a final concentration of 33 μmol/L. The remaining protein extract with Bio-Isoxazole was then incubated at 4°C with slow rotation for 1 hour. The precipitated protein was collected by centrifugation at 14,000 × *g* for 5 minutes, and 50 μL of the supernatant was then taken out as supernatant. Precipitated protein was then washed with 0.1% NP-40 extraction buffer 2 times with centrifugation at 14,000 × *g* for 5 minutes. Then 2× laemmli buffer with 5% beta-mercaptoethanol (Bio-Rad) was used to dissolve the protein precipitation with heating at 95°C for 5 minutes. An equal volume of 2× laemmli buffer was added to the input and supernatant samples and boiled at 95°C for 5 minutes. Boiled protein samples were then used in PAGE gel separation and immunoblot analysis.

PDX Model for Drug Combination Treatment

Primary AML samples were slowly thawed by adding PBS + 1% BSA. Cells were collected and injected through the tail vein into the NSGS mice [*NOD.Cg-Prkdc^{scid}; Il2rg^{tm1Wjl}; Tg(CMV-IL3, CSF2, KITLG)^{1Eav/MloYScJ}*, The Jackson Laboratory], with 5 million live AML blast cells per mouse as described previously (39). Peripheral blood chimerism was monitored by the percentage of human CD45 staining (BioLegend anti-human CD45 BV405). When peripheral blood chimerism reached 2%, treatment was initiated with the following scheme: vehicle (5% Kolliphor, 20% 2-Hydroxypropyl-β-cyclodextrin) every day (q.d.); 10 mg/kg eltanexor (purchased from ApexBio, B8335, dissolved in 0.5% hypromellose, 1% Tween 80) q.d.; 80 mg/kg MI-3454 (synthesized in-house, dissolved in 5% Kolliphor, 20% 2-Hydroxypropyl-β-cyclodextrin) q.d.; and combination of 10 mg/kg eltanexor and 80 mg/kg MI-3454 two times a day by gavage feeding. Treatment was continued for 28 days. Body weight of the animals was monitored during treatment. If the animals experienced a significant body weight loss (over 2 g) or showed signs of discomfort like reduction in activity, drug treatment was stopped for 1 to 2 days to allow the animal to recover body weight. Then peripheral blood chimerism was again analyzed at 2 weeks and 4 weeks after treatment by flow cytometry analysis of hCD45 staining. The mouse work was performed under the oversight of the University Committee on Use and Care of Animals at the University of Michigan with an Institutional Animal Care and Use Committee-approved animal protocol.

Coimmunoprecipitation

Coimmunoprecipitation (Co-IP) was performed using the Nuclear Complex Co-IP Kit (Active Motif, 54001) following the manufacturer's manual. Briefly, 1–2 × 10⁷ OCI-AML3 cells were harvested with or without 10 minutes of 1% formaldehyde fixation. Extraction of chromatin protein by a shearing enzyme in the kit was performed at 4°C with slow rotation for 1 hour. Co-IP of XPO1 and NPM1c were performed with IP high buffer overnight at 4°C. Magnetic protein A beads (Thermo

Scientific, 88846) were then added to Co-IP solution for 2 hours. Beads were washed with IP high buffer 3 times. Enriched interacting protein was eluted by heating the beads in 2× laemmli buffer (Bio-Rad) at 95°C for 5 minutes. To avoid the strong interference of IgG heavy chain in immunoblot detection, light-chain-specific Mouse Anti-rabbit IgG (Cell Signaling Technology, cat. #45262, RRID:AB_2799281) was used to detect NPM1c in the immunoblot after Co-IP.

Antibodies used in Co-IP included NPM1c (Novus Biologicals, Rabbit Polyclonal, NB110-61646, RRID:AB_964800) and XPO1 (Novus Biologicals, Rabbit Polyclonal, NB100-79802, RRID:AB_2215823).

Data Availability

All CUT&RUN, ChIP-seq, RNA-seq, and Bru-seq data have been deposited to the Gene Expression Omnibus under accession GSE197387 (<https://www.ncbi.nlm.nih.gov/geo/query/acc.cgi?acc=GSE197387>).

Authors' Disclosures

T. Cierpicki reports other support from Kura Oncology during the conduct of the study; grants and other support from the NIH outside the submitted work; and a patent for 16/082,645 issued, licensed, and with royalties paid from Kura Oncology. J. Grembecka reports other support from Kura Oncology and grants from the NIH (1R01CA160467 and 1R01CA201204) during the conduct of the study, as well as a patent for 16/082,645 issued, licensed, and with royalties paid from Kura Oncology. S. Chong reports grants from the Shurl and Kay Curci Foundation, The Pew Charitable Trusts, the Kinship Foundation, and the Merkin Institute for Translational Research during the conduct of the study. L. Wan reports serving as a consultant for Bridge Medicines. X. Zhang reports grants from the American Society of Hematology and EvansMDS research foundation during the conduct of the study. No disclosures were reported by the other authors.

Authors' Contributions

X.Q.D. Wang: Conceptualization, data curation, validation, investigation, visualization, methodology, writing—original draft, project administration. **D. Fan:** Data curation, formal analysis, investigation. **Q. Han:** Data curation, software, formal analysis. **Y. Liu:** Investigation. **H. Miao:** Investigation. **X. Wang:** Data curation, visualization. **Q. Li:** Data curation. **D. Chen:** Investigation. **H. Gore:** Investigation, methodology. **P. Himadewi:** Data curation. **G.P. Pfeifer:** Writing—review and editing. **T. Cierpicki:** Resources, supervision. **J. Grembecka:** Resources, supervision. **J. Su:** Data curation, software, supervision, writing—original draft, project administration. **S. Chong:** Data curation, supervision, visualization, writing—original draft, writing—review and editing. **L. Wan:** Supervision, writing—original draft, project administration, writing—review and editing. **X. Zhang:** Conceptualization, data curation, formal analysis, supervision, funding acquisition, investigation, visualization, methodology, writing—original draft, project administration, writing—review and editing.

Acknowledgments

We thank Dr. Margaret Goodell for her support of this work by sharing the OCI-AML3 NPM1c degron 2 cell line. We also thank Dr. Michael Gundry and Dr. Lorenzo Brunetti for their valuable suggestions during the discussion at the early phase of this project. We thank Dr. Chao Lu, Dr. Jia Fei, and Dr. Tianpeng Gu for their vibrant discussion on this project. We also thank Yushuai Liu and Shan Tang for their support on microscopy imaging and immunofluorescence. X. Zhang was supported by an American Society of Hematology Fellow Award and an EvansMDS research foundation Young Investigator Award during the execution of the project. T. Cierpicki is supported by the NIH/NCI (R01CA207272 and R01CA240514). J. Grembecka is supported by NIH/NCI

(R01CA160467). L. Wan is supported by an NIH Director's New Innovator Award (1DP2HG012443), an NIH Pathway to Independence Award (R00CA226399), the Pew-Stewart Scholars Program for Cancer Research, a V Foundation Scholar Award, and an American Society of Hematology Scholar Award. Y. Liu is supported by an Abramson Family Cancer Research Institute Postdoctoral Fellowship. S. Chong is supported by a Shurl and Kay Curci Foundation Research Grant, the Pew-Stewart Scholars Program for Cancer Research (00036068), the Searle Scholars Program (SSP-2022-108), and a Merkin Innovation Seed Grant.

The publication costs of this article were defrayed in part by the payment of publication fees. Therefore, and solely to indicate this fact, this article is hereby marked "advertisement" in accordance with 18 USC section 1734.

Note

Supplementary data for this article are available at Cancer Discovery Online (<http://cancerdiscovery.aacrjournals.org/>).

Received April 15, 2022; revised September 15, 2022; accepted November 30, 2022; published first December 1, 2022.

REFERENCES

- Brunetti L, Gundry MC, Goodell MA. New insights into the biology of acute myeloid leukemia with mutated NPM1. *Int J Hematol* 2019;110:150–60.
- Falini B, Brunetti L, Sportoletti P, Martelli MP. NPM1-mutated acute myeloid leukemia: from bench to bedside. *Blood* 2020;136:1707–21.
- Falini B, Nicoletti I, Martelli MF, Mecucci C. Acute myeloid leukemia carrying cytoplasmic/mutated nucleophosmin (NPMc+ AML): biology and clinical features. *Blood* 2007;109:874–85.
- Grisendi S, Mecucci C, Falini B, Pandolfi PP. Nucleophosmin and cancer. *Nat Rev Cancer* 2006;6:493–505.
- Scott DD, Oeffinger M. Nucleolin and nucleophosmin: nucleolar proteins with multiple functions in DNA repair. *Biochem Cell Biol* 2016;94:419–32.
- Wang W, Budhu A, Forgues M, Wang XW. Temporal and spatial control of nucleophosmin by the Ran-Crm1 complex in centrosome duplication. *Nat Cell Biol* 2005;7:823–30.
- Mitrea DM, Cika JA, Stanley CB, Nourse A, Onuchic PL, Banerjee PR, et al. Self-interaction of NPM1 modulates multiple mechanisms of liquid-liquid phase separation. *Nat Commun* 2018;9:842.
- Feric M, Vaidya N, Harmon TS, Mitrea DM, Zhu L, Richardson TM, et al. Coexisting liquid phases underlie nucleolar subcompartments. *Cell* 2016;165:1686–97.
- Falini B, Mecucci C, Tiacci E, Alcalay M, Rosati R, Pasqualucci L, et al. Cytoplasmic nucleophosmin in acute myelogenous leukemia with a normal karyotype. *N Engl J Med* 2005;352:254–66.
- Spencer DH, Young MA, Lamprecht TL, Helton NM, Fulton R, O'Laughlin M, et al. Epigenomic analysis of the HOX gene loci reveals mechanisms that may control canonical expression patterns in AML and normal hematopoietic cells. *Leukemia* 2015;29:1279–89.
- Uckelmann HJ, Kim SM, Wong EM, Hatton C, Giovinazzo H, Gadrey JY, et al. Therapeutic targeting of preleukemia cells in a mouse model of NPM1 mutant acute myeloid leukemia. *Science* 2020;367:586–90.
- Vassiliou GS, Cooper JL, Rad R, Li J, Rice S, Uren A, et al. Mutant nucleophosmin and cooperating pathways drive leukemia initiation and progression in mice. *Nat Genet* 2011;43:470–5.
- Cheng K, Sportoletti P, Ito K, Clohessy JG, Teruya-Feldstein J, Kutok JL, et al. The cytoplasmic NPM mutant induces myeloproliferation in a transgenic mouse model. *Blood* 2010;115:3341–5.
- Sportoletti P, Grisendi S, Majid SM, Cheng K, Clohessy JG, Viale A, et al. Npm1 is a haploinsufficient suppressor of myeloid and lymphoid malignancies in the mouse. *Blood* 2008;111:3859–62.
- Grisendi S, Bernardi R, Rossi M, Cheng K, Khandker L, Manova K, et al. Role of nucleophosmin in embryonic development and tumorigenesis. *Nature* 2005;437:147–53.
- Gu X, Ebrahmq Q, Mahfouz RZ, Hasipek M, Enane F, Radivoyevitch T, et al. Leukemogenic nucleophosmin mutation disrupts the transcription factor hub that regulates granulomonocytic fates. *J Clin Invest* 2018;128:4260–79.
- Wang AJ, Han Y, Jia N, Chen P, Minden MD. NPM1c impedes CTCF functions through cytoplasmic mislocalization in acute myeloid leukemia. *Leukemia* 2020;34:1278–90.
- Wu HC, Rerolle D, Berthier C, Hleihel R, Sakamoto T, Quentin S, et al. Actinomycin D targets NPM1c-primed mitochondria to restore PML-driven senescence in AML therapy. *Cancer Discov* 2021;11:3198–213.
- Escobar TM, Yu JR, Liu S, Lucero K, Vasilyev N, Nudler E, et al. Inheritance of repressed chromatin domains during S phase requires the histone chaperone NPM1. *Sci Adv* 2022;8:eabm3945.
- Qin G, Wang X, Ye S, Li Y, Chen M, Wang S, et al. NPM1 upregulates the transcription of PD-L1 and suppresses T cell activity in triple-negative breast cancer. *Nat Commun* 2020;11:1669.
- Lin J, Kato M, Nagata K, Okuwaki M. Efficient DNA binding of NF-kappaB requires the chaperone-like function of NPM1. *Nucleic Acids Res* 2017;45:3707–23.
- Oka M, Mura S, Otani M, Miyamoto Y, Nogami J, Maehara K, et al. Chromatin-bound CRM1 recruits SET-Nup214 and NPM1c onto HOX clusters causing aberrant HOX expression in leukemia cells. *Elife* 2019;8:e46667.
- Brunetti L, Gundry MC, Sorcini D, Guzman AG, Huang YH, Ramabadran R, et al. Mutant NPM1 maintains the leukemic state through HOX expression. *Cancer Cell* 2018;34:499–512.
- Dawson MA, Gudgin EJ, Horton SJ, Giotopoulos G, Meduri E, Robson S, et al. Recurrent mutations, including NPM1c, activate a BRD4-dependent core transcriptional program in acute myeloid leukemia. *Leukemia* 2014;28:311–20.
- Zhang W, Zhao C, Zhao J, Zhu Y, Weng X, Chen Q, et al. Inactivation of PBX3 and HOXA9 by down-regulating H3K79 methylation represses NPM1-mutated leukemic cell survival. *Theranostics* 2018;8:4359–71.
- Loven J, Hoke HA, Lin CY, Lau A, Orlando DA, Vakoc CR, et al. Selective inhibition of tumor oncogenes by disruption of super-enhancers. *Cell* 2013;153:320–34.
- Whyte WA, Orlando DA, Hnisz D, Abraham BJ, Lin CY, Kagey MH, et al. Master transcription factors and mediator establish super-enhancers at key cell identity genes. *Cell* 2013;153:307–19.
- Kerry J, Godfrey L, Repapi E, Tapia M, Blackledge NP, Ma H, et al. MLL-AF4 spreading identifies binding sites that are distinct from super-enhancers and that govern sensitivity to DOT1L inhibition in leukemia. *Cell Rep* 2017;18:482–95.
- Somerville TDD, Simeoni F, Chadwick JA, Williams EL, Spencer GJ, Boros K, et al. Derepression of the irquois homeodomain transcription factor gene IRX3 confers differentiation block in acute leukemia. *Cell Rep* 2018;22:638–52.
- Grummitt CG, Townsley FM, Johnson CM, Warren AJ, Bycroft M. Structural consequences of nucleophosmin mutations in acute myeloid leukemia. *J Biol Chem* 2008;283:23326–32.
- Janicki SM, Tsukamoto T, Salghetti SE, Tansey WP, Sachidanandam R, Prasanth KV, et al. From silencing to gene expression: real-time analysis in single cells. *Cell* 2004;116:683–98.
- Wan L, Chong S, Xuan F, Liang A, Cui X, Gates L, et al. Impaired cell fate through gain-of-function mutations in a chromatin reader. *Nature* 2020;577:121–6.
- Chong S, Dugast-Darzacq C, Liu Z, Dong P, Dailey GM, Cattoglio C, et al. Imaging dynamic and selective low-complexity domain interactions that control gene transcription. *Science* 2018;361:eaar2555.
- Johnson KD, Kong G, Gao X, Chang YI, Hewitt KJ, Sanalkumar R, et al. Cis-regulatory mechanisms governing stem and progenitor cell transitions. *Sci Adv* 2015;1:e1500503.
- Groschel S, Sanders MA, Hoogenboezem R, de Wit E, Bouwman BAM, Erpelinck C, et al. A single oncogenic enhancer rearrangement causes concomitant suppressor of EVI1 and GATA2 deregulation in leukemia. *Cell* 2014;157:369–81.
- Grass JA, Jing H, Kim SI, Martowicz ML, Pal S, Blobel GA, et al. Distinct functions of dispersed GATA factor complexes at an endogenous gene locus. *Mol Cell Biol* 2006;26:7056–67.

37. Oka M, Mura S, Yamada K, Sangel P, Hirata S, Maehara K, et al. Chromatin-prebound Crm1 recruits Nup98-HoxA9 fusion to induce aberrant expression of Hox cluster genes. *Elife* 2016;5:e09540.
38. Klossowski S, Miao H, Kempinska K, Wu T, Purohit T, Kim E, et al. Menin inhibitor MI-3454 induces remission in MLL1-rearranged and NPM1-mutated models of leukemia. *J Clin Invest* 2020;130:981–97.
39. Kuhn MW, Song E, Feng Z, Sinha A, Chen CW, Deshpande AJ, et al. Targeting chromatin regulators inhibits leukemogenic gene expression in NPM1 mutant leukemia. *Cancer Discov* 2016;6:1166–81.
40. Camus V, Miloudi H, Taly A, Sola B, Jardin F. XPO1 in B cell hematological malignancies: from recurrent somatic mutations to targeted therapy. *J Hematol Oncol* 2017;10:47.
41. Azmi AS, Uddin MH, Mohammad RM. The nuclear export protein XPO1 - from biology to targeted therapy. *Nat Rev Clin Oncol* 2021;18:152–69.
42. Etchin J, Berezovskaya A, Conway AS, Galinsky IA, Stone RM, Baloglu E, et al. KPT-8602, a second-generation inhibitor of XPO1-mediated nuclear export, is well tolerated and highly active against AML blasts and leukemia-initiating cells. *Leukemia* 2017;31:143–50.
43. Horman SR, Velu CS, Chaubey A, Bourdeau T, Zhu J, Paul WE, et al. Gfi1 integrates progenitor versus granulocytic transcriptional programming. *Blood* 2009;113:5466–75.
44. Chong S, Graham TGW, Dugast-Darzacq C, Dailey GM, Darzacq X, Tjian R. Tuning levels of low-complexity domain interactions to modulate endogenous oncogenic transcription. *Mol Cell* 2022;82:2084–97.
45. Trojanowski J, Frank L, Rademacher A, Mucke N, Grigaitis P, Rippe K. Transcription activation is enhanced by multivalent interactions independent of phase separation. *Mol Cell* 2022;82:1878–93.
46. Song L, Yao X, Li H, Peng B, Boka AP, Liu Y, et al. Hotspot mutations in the structured ENL YEATS domain link aberrant transcriptional condensates and cancer. *Mol Cell* 2022;82:4080–98.
47. Loberg MA, Bell RK, Goodwin LO, Eudy E, Miles LA, SanMiguel JM, et al. Sequentially inducible mouse models reveal that Npm1 mutation causes malignant transformation of Dnmt3a-mutant clonal hematopoiesis. *Leukemia* 2019;33:1635–49.
48. Yun H, Narayan N, Vohra S, Giotopoulos G, Mupo A, Madrigal P, et al. Mutational synergy during leukemia induction remodels chromatin accessibility, histone modifications and three-dimensional DNA topology to alter gene expression. *Nat Genet* 2021;53:1443–55.
49. Rau R, Magoon D, Greenblatt S, Li L, Annesley C, Duffield AS, et al. NPMc+ cooperates with Flt3/ITD mutations to cause acute leukemia recapitulating human disease. *Exp Hematol* 2014;42:101–13.
50. Li H, Handsaker B, Wysoker A, Fennell T, Ruan J, Homer N, et al. The sequence alignment/map format and SAMtools. *Bioinformatics* 2009;25:2078–9.
51. Zhang Y, Liu T, Meyer CA, Eeckhoutte J, Johnson DS, Bernstein BE, et al. Model-based analysis of ChIP-Seq (MACS). *Genome Biol* 2008;9:R137.
52. Shao Z, Zhang Y, Yuan GC, Orkin SH, Waxman DJ. MANorm: a robust model for quantitative comparison of ChIP-Seq data sets. *Genome Biol* 2012;13:R16.
53. Himadewi P, Wang XQD, Feng F, Gore H, Liu Y, Yu L, et al. 3'HS1 CTCF binding site in human beta-globin locus regulates fetal hemoglobin expression. *Elife* 2021;10:e70557.
54. Dobin A, Davis CA, Schlesinger F, Drenkow J, Zaleski C, Jha S, et al. STAR: ultrafast universal RNA-seq aligner. *Bioinformatics* 2013;29:15–21.
55. Li B, Dewey CN. RSEM: accurate transcript quantification from RNA-Seq data with or without a reference genome. *BMC Bioinf* 2011;12:323.
56. Love MI, Huber W, Anders S. Moderated estimation of fold change and dispersion for RNA-seq data with DESeq2. *Genome Biol* 2014;15:550.
57. Paulsen MT, Veloso A, Prasad J, Bedi K, Ljungman EA, Tsan YC, et al. Coordinated regulation of synthesis and stability of RNA during the acute TNF-induced proinflammatory response. *Proc Natl Acad Sci U S A* 2013;110:2240–5.
58. Wang J, Zhao Y, Zhou X, Hiebert SW, Liu Q, Shyr Y. Nascent RNA sequencing analysis provides insights into enhancer-mediated gene regulation. *BMC Genomics* 2018;19:633.
59. Herrmann C, Avgousti DC, Weitzman MD. Differential salt fractionation of nuclei to analyze chromatin-associated proteins from cultured mammalian cells. *Bio Protoc* 2017;7:e2175.
60. Skene PJ, Henikoff S. An efficient targeted nuclease strategy for high-resolution mapping of DNA binding sites. *Elife* 2017;6:e21856.